EFFECT OF FORMING SPEEDS ON COIL-BREAK FORMATION DURING UNCOILING OF FULLY ANNEALED LOW CARBON STEEL SHEETS – A 3D FINITE ELEMENT SIMULATION STUDY

KAM WENG JOE

FACULTY OF ENGINEERING
UNIVERSITY OF MALAYA
KUALA LUMPUR

2022

EFFECT OF FORMING SPEEDS ON COIL-BREAK FORMATION DURING UNCOILING OF FULLY ANNEALED LOW CARBON STEEL SHEETS – A 3D FINITE ELEMENT SIMULATION STUDY

KAM WENG JOE

RESEARCH REPORT SUBMITTED TO THE FACULTY OF ENGINEERING UNIVERSITY MALAYA, IN PARTIAL FULFILMENT OF THE REQUIREMENTS FOR THE DEGREE OF MASTER OF MECHANICAL ENGINEERING

2022

UNIVERSITY OF MALAYA

ORIGINAL LITERARY WORK DECLARATION

Name of Candidate: **KAM WENG JOE**

Matric No: **S2037435**

Name of Degree: **MASTER OF MECHANICAL ENGINEERING**

Title of Project Paper/Research Report/Dissertation/Thesis ("this Work"): **EFFECT OF FORMING SPEEDS ON COIL-BREAK FORMATION DURING UNCOILING OF FULLY ANNEALED LOW CARBON STEEL SHEETS- A 3D FINITE ELEMENT SIMULATION STUDY**

Field of Study: **Sheet Metal Forming**

I do solemnly and sincerely declare that:

(1) I am the sole author/writer of this Work;
(2) This Work is original;
(3) Any use of any work in which copyright exists was done by way of fair dealing and for permitted purposes and any excerpt or extract from, or reference to or reproduction of any copyright work has been disclosed expressly and sufficiently and the title of the Work and its authorship have been acknowledged in this Work;
(4) I do not have any actual knowledge nor do I ought reasonably to know that the making of this work constitutes an infringement of any copyright work;
(5) I hereby assign all and every rights in the copyright to this Work to the University of Malaya ("UM"), who henceforth shall be owner of the copyright in this Work and that any reproduction or use in any form or by any means whatsoever is prohibited without the written consent of UM having been first had and obtained;
(6) I am fully aware that if in the course of making this Work I have infringed any copyright whether intentionally or otherwise, I may be subject to legal action or any other action as may be determined by UM.

Candidate's Signature Date: 23/2/2022

Subscribed and solemnly declared before,

Witness's Signature Date: 23/2/2022

Name: Dr Tan Chin Joo

Designation: Supervisor

[EFFECT OF FORMING SPEEDS ON COIL BREAK FORMATION DURING UNCOILING OF FULLY ANNEALED LOW CARBON STEEL SHEETS – A 3D FINITE ELEMENT SIMULATION STUDY]

ABSTRACT

Coil breaks are narrow, irregularly changing deformation lines that causes difficulties in many steel industries as it is considered as a serious surface defect which leads to esthetical problems on the final product. A 3D explicit finite element model was developed to evaluate the coil break formations during uncoiling of full annealed low carbon steel sheets at different speeds. The 3D model consists of 2 lap coils measuring 600 mm in the inner core diameter and 300 mm width with a sheet thickness of 1.5 mm. The line speed was increased from 1 mpm to 1000 mpm and the change in true (LE11) strains and stress distributions (S11) along the longitudinal direction on top surface of the sheet were recorded. The simulation results show that there are 7 interruption zones with Zone A consists of narrow band of compressive strain and Zone B which consists of islands of tensile strain or coil breaks. The strain rate of the uninterrupted element increased the highest from 0.0007 to 1.1920 /s when the uncoiling speed increased from 1 mpm to 1000 mpm. The higher strain rate will cause the LE11 to reduce which minimizes the peak height. Hence, coil break was able to minimize with 1000 mpm as it subjected to a higher strain rate. Coil tensions were varied from 36 N/mm to 176 N/mm to further reduced the coil break with 1000 mpm line speed. 1000 mpm with coil tension of 146 N/mm was selected as the optimum profile as the severity of the coil breaks are the lowest. In the mesh analysis using higher integration points, the formation of coil break in Zone B1 were eliminated and the severity of coil breaks were increased as more accurate results were obtained. The total computational time recorded for 1000 mpm with coil tension of 146 N/mm with 7 integration points was 0.38 hours (22.8 minutes).

Keywords: Coil breaks, edge breaks, low carbon steel sheet, finite element simulation

[EFFECT OF FORMING SPEEDS ON COIL BREAK FORMATION DURING UNCOILING OF FULLY ANNEALED LOW CARBON STEEL SHEETS – A 3D FINITE ELEMENT SIMULATION STUDY]

ABSTRAK

Pemutus gegelung adalah garisan-garisan cacat yang serius dan sempit yang menyebabkan kesukaran dalam industri keluli. Model elemen 3D eksplisit telah dibangunkan untuk menilai pembentukan pemutus gegelung ketika proses membuka lingkaran lembaran keluli kawat-ikat berkarbon rendah pada kelajuan yang berbeza. Model 3D terdiri daripada 2 gegelung tindih berukuran 600 mm bagi diameter teras dalaman dan 300 mm lebar dengan ketebalan lembaran 1.5 mm. Kelajuan pemebentukan ditingkatkan dari 1 kepada 1000 mpm, dan perubahan dalam kekangan (LE11) dan penyebaran tekanan (S11) di permukaan atas direkodkan. Keputusan simulasi menunjukkan 7 zon gangguan, dengan Zon A yang terdiri daripada jalur sempit terikan mampat dan Zon B, yang terdiri daripada pemutus gegelung. Kadar terikan unsur tanpa gangguan meningkat paling tinggi daripada 0.0007 kepada 1.1920/s apabila kelajuan uncoiling meningkat daripada 1 mpm kepada 1000 mpm. Kadar terikan yang lebih tinggi akan menyebabkan LE11 berkurangan yang meminimumkan ketinggian puncak. Oleh itu, pemutus gegelung telah diminimumkan dengan 1000 mpm kerana ia tertakluk kepada kadar terikan yang lebih tinggi. Ketegangan gegelung berbeza dari 36 hingga 176 N/mm untuk mengurangkan lagi pemutus gegelung dengan kelajuan pembentukan 1000 mpm. 1000 mpm dengan ketegangan gegelung 146 N/mm dipilih sebagai profil optimum kerana tahap pemutus gegelung adalah yang paling rendah. Dalam analisis jejaring menggunakan titik integrasi yang lebih tinggi, pembentukan pemutus gegelung di Zon B1 telah dihapuskan. Jumlah masa pengiraan yang direkodkan untuk 1000 mpm dengan 146 N/mm dengan 7 titik integrasi adalah 0.38 jam (22.8 minit).

Kata kunci: Pemutus gegelung, pemutus tepi, lembaran keluli karbon rendah, simulasi

ACKNOWLEDGEMENTS

It is always a pleasure to remind the fine people in the UNIVERISTY OF MALAYA for their sincere guidance that I received to uphold my Master's degree study.

Foremost, I would like to express my sincere gratitude to my advisor Dr Tan Chin Joo for the continuous support of my research, for his patience, motivation, enthusiasm, and immense knowledge. His guidance helped me in all the time of research and writing of this thesis. I could not have imagined having a better advisor and mentor for my research project.

Secondly, I would like to thank my parents, for giving birth to me in the first place and supporting me spiritually throughout my life.

Finally, I apologize to all other unnamed who help me in various ways to have good training.

TABLE OF CONTENTS

LIST OF FIGURES

LIST OF TABLES

LIST OF SYMBOLS AND ABBREVIATIONS

ACB	:	Anti Coil Break
AISI	:	American Iron and Steel Institute
ASTM	:	American Society for Testing and Materials
CAE	:	Computer Aided Engineering
FE	:	Finite Element
HSLA	:	High Strength Low Alloy Steels
LCS	:	Low Carbon Steel
LE11	:	Logarithmic strain on the x-axis face in the x-direction
MPM	:	Meter per minute
MS	:	Mass scaled
S11	:	True stress on the x-axis in the x-direction
STL	:	Skin-pass Tension Line
TB	:	Backward Tension
TF	:	Forward Tension
YPE	:	Yield Point Elongation

CHAPTER 1: INTRODUCTION

1.1 Background

Low carbon steel (LCS) is the most widely used form of carbon steel in the oil and gas industry sectors. They are excellent for machining and wielding with low cost due to their high ductility. Examples of applications of it are such as the automobile body components, structural shapes (I-beams), pipes, construction, and bridge components. However, surface defects such as coil break are commonly found in the acid pickling, cold rolling and cutting line which leads to esthetical problems on the final product. This often does not meet the customer requirement and leads to lower productivity in production line. In the previous study by Tan and Liew (2021), a 3D finite element (FE) model based on the implicit method was developed. The effect of the coil forward tension and the application of anti-coil break (ACB) roll on the formation of coil-break during uncoiling of full-annealed LCS sheets were investigated using a non-linear quasi-static stress analysis. It was reported that a coil forward tension of 166N/m with ACB roll was able to reduce the coil break formation by 30%.

In this study, the effect of forming speeds (m/min) and number of integration points in the thickness direction on coil break formation will be investigated using a developed 3D simulation model based on explicit dynamic method.

1.2 Problem Statements

Coil breaks are irregularly changing plastic deformed bands on the surface of low carbon steel strips due to incomplete bending during uncoiling. This often does not meet the customer requirement for high surface quality and resulted in a lower product price. The break marks can be attributed to many parameters such as uncoiling speed, coiling temperature, mechanical alignment of equipment, annealing and coil tension. However, it is difficult to completely remove the coil break marks, as it is inherent in the low carbon

steel. Although the severity and intensity of the coil breaks marks can be reduced with secondary processes such as skin pass rolling, it can cause additional costs and reduced productivity in the manufacturing line. Therefore, it is important to remove the coil break formations in the early stage to prevent it from propagating later to save cost. At present, there is only a few literature studies about the formation of coil break. The occurrence frequency of this surface defect is high in production and significantly impacts the strip quality. Hence, it is vital to conduct an in-depth study to investigate and analyzed the coil break formations prior secondary processes to improve the surface quality of strip and to increase market competitiveness.

1.3 Objectives of study

1. To develop a 3D simulation model based on dynamic explicit method for the uncoiling process of fully annealed low carbon steel sheets
2. To investigate the effect of forming speeds (m/min) and integration points on coil-break formation along the uncoiled sheet surfaces
3. To minimize the degree of coil-break formation during the uncoiling process

1.4 Scope of study

This study is focused on developing a 3D simulation model based on explicit method with Abaqus/CAE software to simulate the uncoiling process at the entry points of the Skin-pass Tension Levelling Line (STL) based on real-life industrial operation system. The formations of coil break on fully annealed LCS sheets during the uncoiling process were investigated by evaluating the logarithmic strain (LE11) peak with the effect of forming speeds of 1, 10, 100 and 1000 m/min. Coil forward tension were varied with value of 36 to 176 N/mm to reduce the severity of break marks. The number of integration points of 3, 5 and 7 in the thickness direction of the sheet model were also analyzed to determine the effect on simulation accuracy and computational time.

1.5 Limitations of study

This research study is limited as the lap coil sheets were reduced for reduction of simulation and computational cost due to Abaqus/CAE has a node limit of 250,000 nodes for meshing. Mass scaling was required to compute the simulation results for 1 mpm as the total computational time required is more than 1 day with large file size data. Furthermore, the results are only valid for sheet thickness of 1.5 mm in this study whereas the actual sheet thickness in the production line may vary from 0.5 mm to 4 mm.

1.6 Significance of study

The 3D finite element model was created and simulated as a digital representation of the uncoiling process to investigate the effect of forming speeds on coil breaks. This is because conducting experiments of forming speed on a real manufacturing line is impossible or impractical due to the limitation of cost and time. Hence, this study was conducted to obtain the optimum value of coil sheet tensions and line speed in the production line prior secondary processes to prevent or reduce the risks of coil break formations to improve the surface quality of the product. It may reduce the amounts of substandard products and increase the overall product price.

1.7 Research Gap

Past studies have found that, coil break formations are due to many parameters such as hot rolling parameters, chemical composition, coiling temperature, mechanical alignment of equipment, annealing cycle and coil tension. Furthermore, the application of anti-coil break roll was able to minimize the coil breaks as it was used to applied pressure for continuous bending during uncoiling.

However, there is little to none research studies in the recent years that investigate the effect of forming speed on coil break formations as it is very costly to collect the experimental data of forming speed on coil break formations. Thus, this study does not

involve any experimental validation or verification on the 3D finite element model with the real experimental model in the manufacturing line. Wendt et al. (2007) mentioned that forming speed, uncoiling tension and uncoiling geometry could be one of the factors that affect the coil breaks formations. Considering this, this present study focuses on developing a 3D simulation model to investigates the effect of forming speed on coil break formation of fully annealed low carbon steels.

CHAPTER 2: LITERATURE REVIEW

2.1 Low Carbon Steel

Low carbon steel also known as the mild-carbon steel is the most recyclable and commonly used material on the planet with applications in almost every aspect in our lives. It is a type of metal alloy that is made up of a relatively low amount of carbon content of 0.05 to 0.30 wt% and manganese content of 0.40 to 1.50 wt%. In industrial practice, carbon steel (carbon-iron alloy) is usually categorized depending on the amount of carbon content as shown in Figure 2.1.

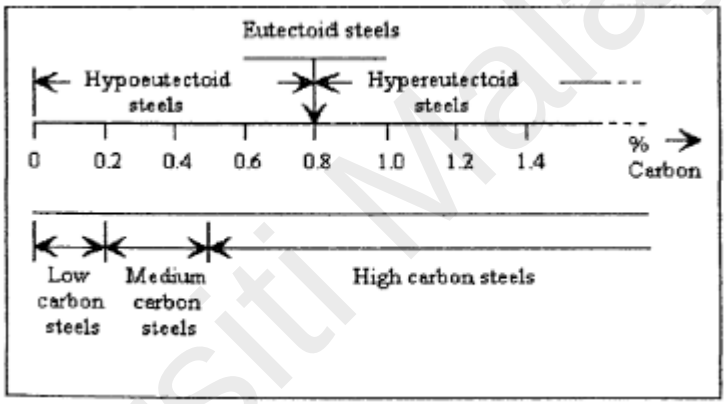

Figure 2.1: Carbon steel classification (Ginzel, 1995)

Moreover, it is a widely used due to its relatively low price with mechanical properties that are favorable in many general-purpose applications. It has unique compatible properties that none other non-ferrous alloy provides such as good machinability, weldability, and formability and high ductility and toughness. Not only that, high strength low-alloy steels (HSLA) are also often categorized as low carbon steels although they contain up to 10 wt% of other alloying elements such as copper, nickel, titanium, vanadium and molybdenum. High strength low-alloy steels are known to have similar properties with plain low carbon steel but with higher strength and good corrosion resistance.

2.2 Applications of Low Carbon Steel

The properties of low carbon steel can be characterized with different amount of carbon content (up to 0.30 wt% of C) depending on its final applications and required mechanical properties as shown in Table 2.1. These material mechanical properties with its low production cost made it suitable for a wide range of applications which includes the construction, transport, appliances, and industry sectors. Low carbon steels were extensively used as building frame, steel cladding, car body frame, pressure vessels and pipelines (Callister & Rethwisch, 2015; David Llewellyn & Roger Hudd, 1998). Upon carburizing, it is also suitable in products such as gear shafts and plunges due to its good ductility and toughness (Islam & Rashed, 2019).

Table 2.1: Applications of low carbon steel (Islam & Rashed, 2019)

AISI grade	Carbon content (wt%)	Yield strength (MPa)	Applications
1010	0.10	180	Automobile panels, wire
1020	0.20	205	Pipes, structural steel, sheet
A36	0.29	220	Structural
A156	0.30	260	Low temperature pressure vessels

2.3 Dynamic tensile properties of Low Carbon Steel

Low carbon steel is a positive sensitive strain rate material. It can be seen in Figure 2.2 that the stress strain curve shift toward the upper left at higher strain rate with high forming speeds which results in increase of yield strength with extended yield point elongation (S. Paul et al., 2014). The occurrence of higher spike height is also found when strain rate increases from 0.0007 to 239 s^{-1}. However, the strain rate usually falls between 0.0007 to 0.7 s^{-1}in the production line of low carbon steel. This is important as

it will determine the ability to predict accurately the behavior of low carbon steel in simulation for more accurate results.

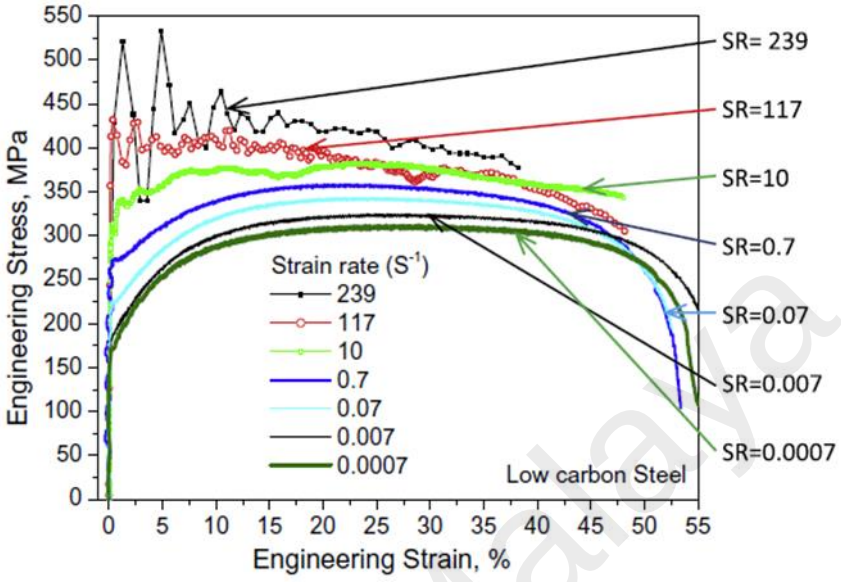

Figure 2.2: Stress strain curve for low carbon steel (S. Paul et al., 2014)

2.4 Rolling Mill

The general production line of the low carbon steel in conventional hot strips mills and secondary process for the cold rolled sheet metals are shown in Figure 2.3. The raw material of LCS is a continuously cast slab which is being preheated to 1240 °C for further plastic deformation. Aluminium-nitride and aluminium-chormium nitride precipitates are usually found in the dissolution of nitrogen at the slab reheating temperature of 1240 °C (A. Mucsi, 2018; S. K. Paul et al., 2011).

Then, the slab is hot rolled to reach the required intermediate strip thickness of 20-30 mm in the austenite region which consists of 6-8 tandem rolls in the roughing mill. The final strip thickness was carried out in the finishing mill with a finishing rolling temperature of 840-900 ˚C depending on the chemical properties and thickness of the coil. When the metal strip left the last finishing stand, it undergoes an accelerated cooling

to a temperature known as coiling temperature ranging between 550 °C and 750 °C with water jets. The strip metal is then coiled with a coiling equipment and stored in a warehouse for ambient cooling to a temperature of 60˚C for 3 days (A. Mucsi et al.). Hot rolled coils are produced and can be sold separately in cheap cost or procced to other secondary processing lines such as slitting, acid pickling, cold rolling, annealing, and skin passing/temper rolling line for better mechanical properties and surface finish.

Here, surface defects such as coil breaks, wavy edge, ridge buckle and edge break are often present in the coil metal. The difficult part is that initiating point of these surface defects cannot be identified easily with the naked eye not until after the last processing stage of tempering (Zhou et al., 2019). Therefore, it must be removed by slitting or trimming operation as the defects may cause the metal sheet to collapse and rupture in the rolling mill. This leads to a loss of productivity as only 50% of the materials only makes it to the final product whereas the rest are lost in the downstream processing and returned to slab reheating (Asefi et al., 2013).

In the acid pickling line, hot rolled coils were conveyed through hydrochloric acid baths to remove the surface impurities. The is to prevent the rust and scrap covered in the hot rolled strip form hindering its applications. Next, the steel then undergoes cold rolling process where its yield and tensile strength increases with its ductility reduced so the that the material can improves its hardness for deep drawing applications (Beganović et al., 2018). Thus, annealing process is important as it improves the ductile properties which causes the material to become softer. After annealing, the coils then undergo furnace cooling and skin passed for further surface finish improvement.

Lastly, quality assurance is done by surface inspection on top and bottom surface of the metal coils before final packaging and dispatch. This is to prevent net loss sales in the company due to surface defects like zipper cracks, coil breaks, wavy edge, alligatoring

and edge breaks. Thakur et al. (2014) mentioned that the surface quality of the coils can be categorized into standard and diversion. Sheet metal coils which meet the customer requirement (<10% of surface defect) are termed as standard whereas the others termed as diversion.

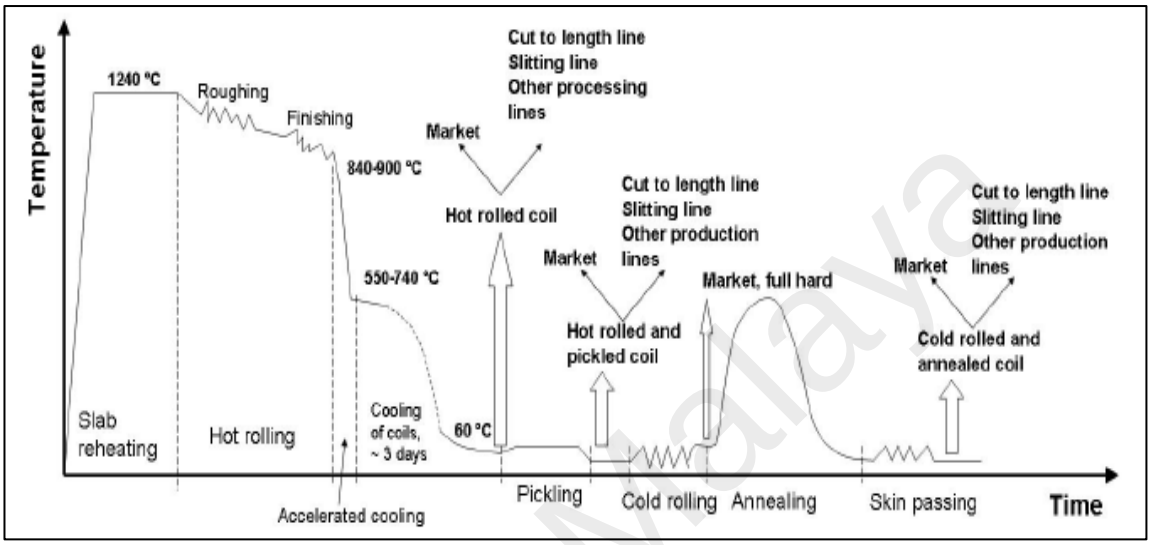

Figure 2.3: Basic production line of low carbon steel strips (A. Mucsi et al.)

2.5 Surface Defects

2.5.1 Wavy edges

Shim et al. (2017) studied the wavy edge formation of corrugated thin-walled sheet metal under large bending deformation as shown in Figure 2.4. It was reported that wavy edges are found when excessive longitudinal compressive stress are applied near the strip edge and localized edge buckling plastic deformation occurs when the bending radius reaches a critical value. In their study, wavy edge formations were successfully minimized by controlling the cross-sectional length of the sheet metal to reduce excessive longitudinal stress.

Figure 2.4: Wavy edges in thin-walled sheet (Shim et al., 2017)

2.5.2 Edge breaks

Zhou et al. (2019) defined edge breaks as edge strains or crease-like defect which are commonly found on steel sheet when exiting the cold milling stage. The appearance of this defect is very similar to coil break, but they are only confined to the edges of the strip. This defect is attributed by an uneven deformation during uncoiling which results the strip coil being stretched beyond its yield point as shown in Figure 2.5.

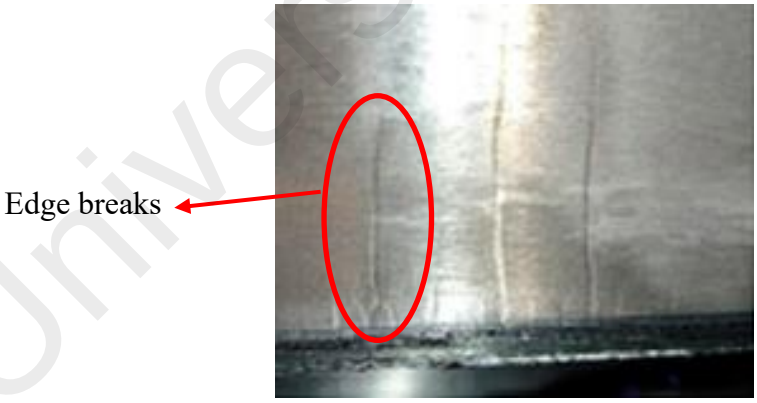

Figure 2.5: Edge breaks in coil strip (Zhou et al., 2019)

2.5.3 Ridge buckle

Sun et al. (2016) defined ridge buckle defect as a bulge that appears on a coil surface which greatly affects the strip quality. This can be attributed due to the accumulation of local wave shapes in cold rolling and uneven residual stress distributions during the coiling process. Usually, buckling plastic deformation occurs first during coiling and cause secondary buildup of small narrow wave shape during uncoiling as shown in Figure 2.6 when the total amount of ridge buckles reaches a certain value. Melfo et al. (2006) demonstrated that ridges are more likely to formed in the last coil strips (> 65 strips rolled) and can be attributed to uneven roll wear due to temperature variations in the strip.

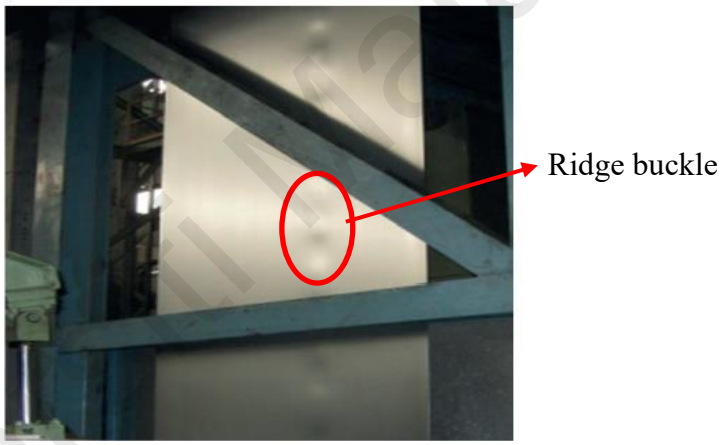

Figure 2.6: Ridge buckle strip after uncoiling (Sun et al., 2016)

2.5.4 Coil breaks

András Mucsi (2018) defined coil breaks as ridges or wrinkles which appear as narrow irregularly parallel deformation lines which extend across the width of metal strip. This surface defect is also known as luders lines, stretcher strains or break marks which attributed to discontinuous yielding phenomenon as shown in Figure 2.7. Normally, coil breaks are aligned in the transverse or rolling direction which extend up to 100 mm across the strip edge and appear in many metallurgical manufacturing stages, such as acid pickling, skin passing, slitting lines, etc. They are a major concern in the surface critical

applications as it is considered as a serious surface defect which leads to esthetical problems on the final product.

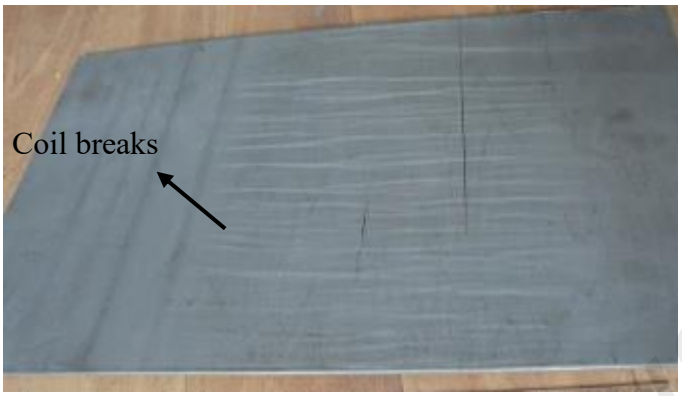

Figure 2.7: Coil breaks in LCS (András Mucsi, 2018)

2.6 Coil break analysis

According to a research done by S. K. Paul et al. (2011), coil break formations were attributed to parameters such as spike height and yield point elongation (YPE). Besides that, Zhou et al. (2019) also stated that coil break formation can be affected by its microstructure, chemical composition, thickness reduction ratio, annealing temperature and grain size.

2.6.1 Spike heights

Spike height is defined as the difference between the upper and lower yield strength and is an important factor of coil break formation (S. K. Paul et al., 2011). In the study, they analyzed the coil break formations by investigating the relationship of spike heights with different coil thickness (1.8, 1.96 and 2.5mm) of Grade 1014 LCS in the acid pickling line. Tensile properties of 12 coil samples with ASTM E8-05 (sheet type) standard was obtained to evaluate the yielding phenomena as depicted in Figure 2.8.

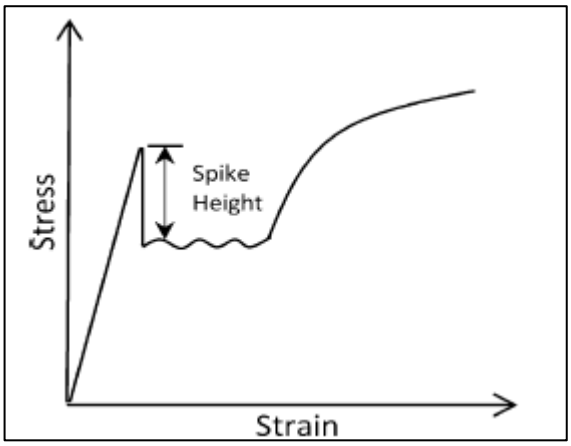

Figure 2.8: Schematic stress-strain diagram (S. K. Paul et al., 2011)

It was shown in Figure 2.9 that the spike height increased with decreasing coil thickness from 2.5 to 1.8mm which caused severe coil break marks. This is due to the finer grain size which caused by the reduction of thickness in hot rolling. Kobayashi (1999) stated that the spike height increases with the upper yield strength can be attributed to grain size. The smaller the grain diameter, resulted in an increase of spike height and upper yield strength. Zhou et al. (2019) explained that recrystallization can be done more readily with a large reduction thickness to obtain finer grain size as more nucleation sites are available during the annealing stage.

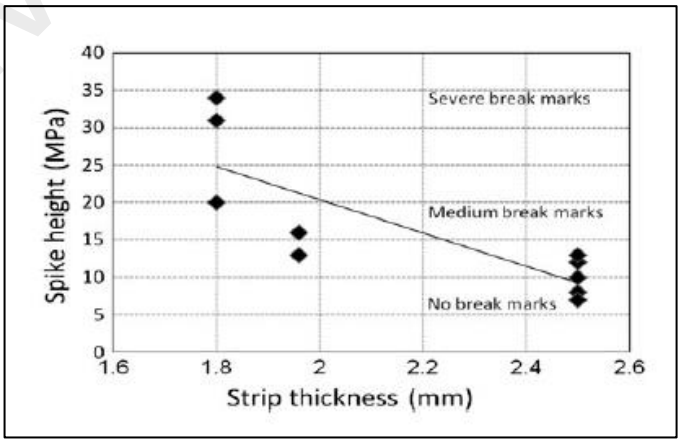

Figure 2.9: Relationship between strip thickness and spike height (S. K. Paul et al., 2011)

2.6.2 Annealing temperature

Annealing is a heat treatment process that heats metal and allows it to cool slowly to reduce hardness, improve ductility and eliminate the internal stresses. Zhou et al. (2019) stated that annealing temperature of 700C was the optimum value to maximize the formation of carbides and nitrides which helps lowering the contents of free interstitial elements such as carbon and nitrogen in the steel matrix. This can also be done by adding elements with high affinity such as Aluminum and Boron to reduce the yield point elongation for reduction of break marks. It was observed in Table 2.2 that low carbon steel samples undergo annealing cycle 2 (700 °C) has a lower yield point when compared to annealing cycle 3 (550 °C).

Table 2.2: YPE with different annealing cycle (Zhou et al., 2019)

AISI grade	Sample	Average diameter (um)	YPE (%)
Annealing cycle 2	0033, Reduction ratio 60%	26.7	0.7
	0033, Reduction ratio 70%	31.8	0.7
Annealing cycle 3	0033, Reduction ratio 80%	13.3	10
	6172, Reduction ratio 60%	44.9	4.5

2.6.3 Grain size

Zhou et al. (2019) reported that grain size has an inverse relationship with yield point elongation (YPE). It can be seen that a larger grain size and structure yields a lower yield point elongation compared to finer grain size as shown in Figure 2.10. Thakur et al. (2014) stated that a larger grain size is necessary for a lower Lüders strains which leads to a reduction of coil break formation. However, S. K. Paul et al. (2011) stated that yield point elongation is not the sole criteria for coil break formation as coil with yield point elongation of (3-4%) did not show any break marks during strip uncoiling. While coils

that shown higher spike heights (>30 MPa) with large yield point elongation have more severe coil breaks.

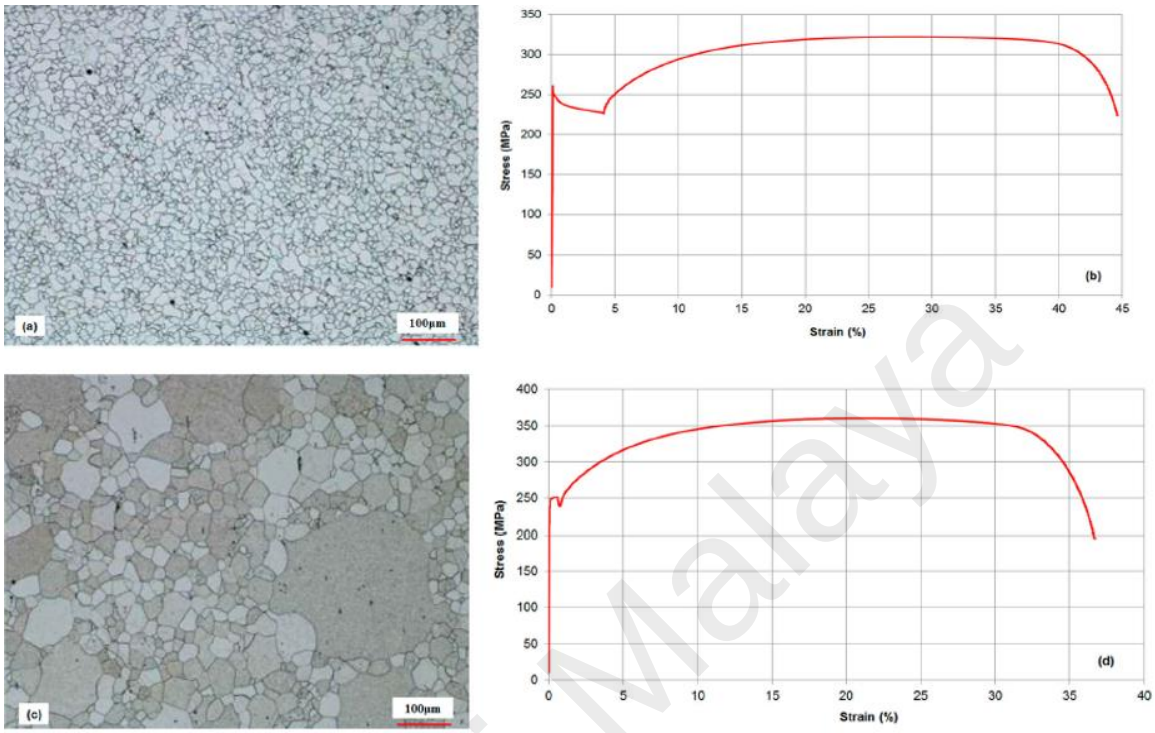

Figure 2.10: Microstructure and stress strain curve using different annealing cycle. (a) Microstructure with annealing cycle 1 (b) microstructure with annealing cycle 2 (c) and d) Stress strain curve (Zhou et al., 2019)

2.6.4 Chemical composition

Zhou et al. (2019) stated that the primary mechanism of Lüders band formation is due to the unpinning of dislocations motion which formed in the interstitial solute atmospheres. This can be attributed by the free interstitial elements such as carbon and nitrogen that form Cottrell atmospheres to pin dislocations over time (Chen, 2008). Thakur et al. (2014) found that coil breaks are more susceptible to occur in higher nitrogen levels of 60 ppm. However, by adding Titanium to minimize the effect of nitrogen yields a similar result with plain carbon steel which indicates the cause of break marks lies elsewhere. S. K. Paul et al. (2011) suggested that the detrimental effect of nitrogen levels only affects the formability of steel but not coil breaks as it resulted in an increased of

yield strength, lower ductility, and toughness and with higher impact transition temperature (ITT).

2.7 Preventions and treatments of coil breaks

2.7.1 Anti-Coil Break (ACB) roll

Tan and Liew (2021) reported that coil break marks can be reduced by 30% with the ACB roller. The objective of the ACB roller was used for continuous bending of the coil sheet. It was found that a low curvature of arc can be seen in Figure 2.11 (b). This is attributed by the compression of the ACB roll which leads to a reduction of tensile strain distributions. Moreover, the details of the backup rolls and ball bearings are important for the ACB roller to be applied correctly. This is to ensure that the applied pressure of the ACB roller is appropriate during the uncoiling process particularly in the ball bearing section. (Mucsi et al., 2016) reported that if ACB roller is not applied properly, it could lead to more coil breaks formations due to excessive applied pressure.

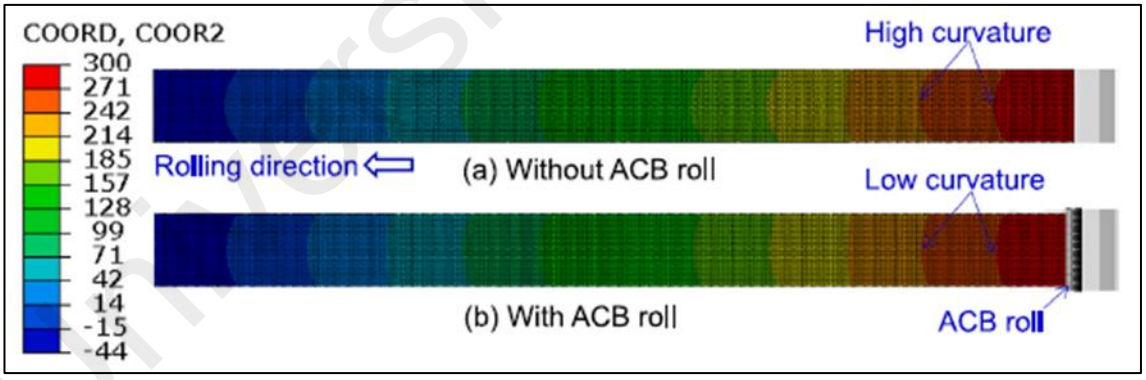

Figure 2.11: Comparison of vertical coordinate distributions during uncoiling (a) without ACB (b) with ACB (Tan & Liew, 2021)

2.7.2 Mechanical alignment of processing equipment

The conditions of the processing equipment are the main contributors to coil breaks. According to Thakur et al. (2014), realignment of bridle roll and uncoiler in the manufacturing production stages led to a significant reduction of break marks from 30% to 2% in the steel manufacturing plant. This is due to the worn out of processing equipment which cause misalignment of (2-5mm) across the width of the coil during uncoiling. By doing monthly maintenance and inspection of processing equipment, coil break formation reduced from 100 tons/ day to 10 tons/day as shown in Figure 2.12.

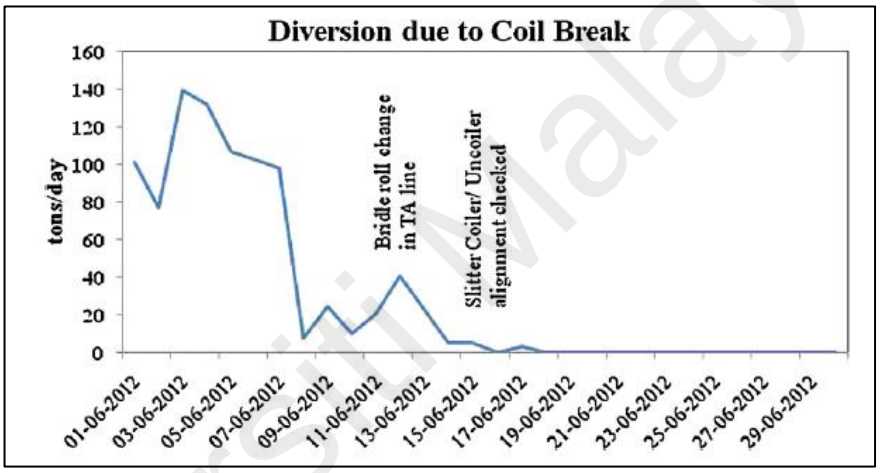

Figure 2.12: Effect of processing equipment on coil break (Thakur et al., 2014)

2.7.3 Temper rolling

Skin-pass rolling known as temper rolling is the final manufacturing stage in metal strip production. Asefi et al. (2013) stated it improves the surface smoothness by introducing a small plastic strain to bypass the discontinuous plastic deformation region and decrease the upper yield point which are attributed by Luder's band effect. According to Beganović et al. (2018), they reported that a skin-pass thickness reduction of 0.5 to 3% leads to the elimination of the local plastic bending of the three-layers strip and coil breaks on the strip surfaces during its uncoiling as shown in Figure 2.13.

Figure 2.13: Different behavior of metal strips (a) during uncoiling and (b) after skin-pass roll (Beganović et al., 2018).

2.7.4 Coil tension

Thakur et al. (2014) noticed that the occurrence of break marks increases with higher coiling tension in the production line. In the study, an optimum coiling tension of 150 kgf was obtained which able to minimize the coil break formations in the production line. Tan and Liew (2021) developed a 3D strip uncoiling simulation model and reported that an optimum coil tension value of 166 N/mm was able to generate less coil breaks as shown in Figure 2.14.

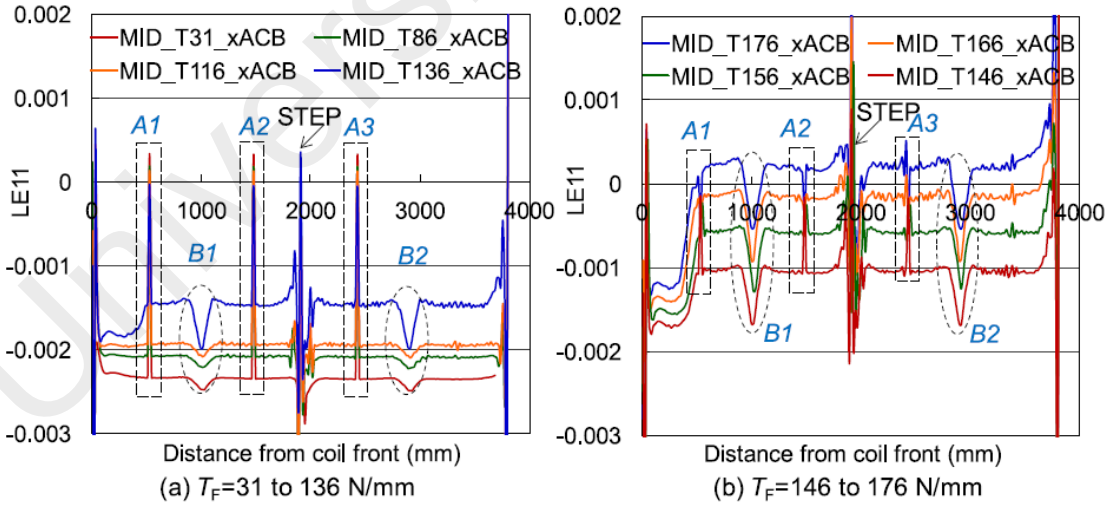

Figure 2.14: Longitudinal strain distributions along middle paths on top surfaces of uncoiled sheets from coil front with increase in coil tension (Tan & Liew, 2021).

CHAPTER 3: METHODOLOGY

3.1 Abaqus/CAE

The general procedures of developing the 3D simulation model can be explained with the flowchart shown in Figure 3.1.

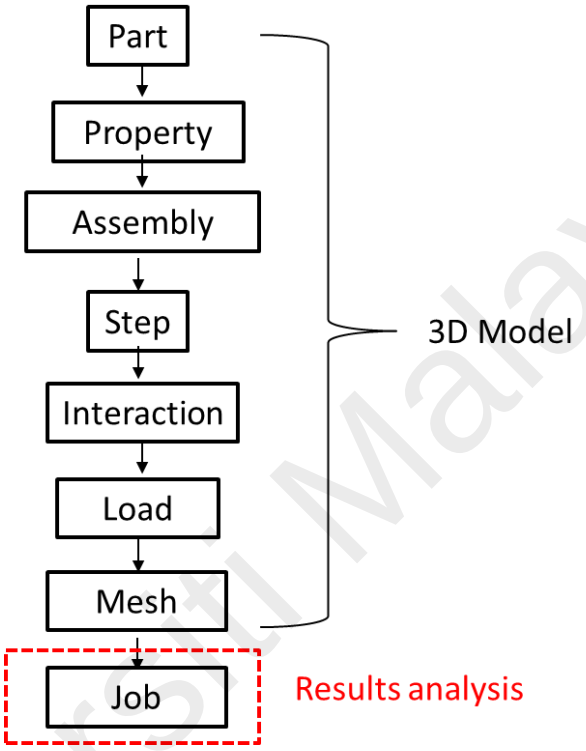

Figure 3.1: Process flowchart of 3D simulation

Firstly, the individual parts of the model are sketched according to their dimensions/geometry. Parts model such as the coil sheet and the uncoiler were created in the part module. Then, sections of the part model were created for its associated material definition/property in the property module. After defining the LCS material property to the coil sheet, the assembly module was carried out to create instances of the parts and to position the instances relative to each other in a global coordinate system for assembly. Interaction between the surfaces of the uncoiler and coil sheet were defined. Boundary conditions and loads such as gravity and external forces were defined in the load module. In order to simulate real life industrial operating systems, analysis steps and its associated

output requests were configured in the step module. After fully defining and developing the model, a finite element mesh was generated to the LCS coil sheet in the mesh module. Lastly, multiple jobs were created for running simulation of the completed model for results analysis.

3.2 Difference between Implicit and Explicit method

Metal sheet forming is a quasi-static process in nature. Although the explicit method is ideally suited for analyzing high speed dynamic problems, many of its advantages are also applicable to the analysis of slower (quasi-static) problems. For example, problems where contact dominates the solution and local instability may form due to wrinkling of sheet metal. The comparisons between implicit and explicit method are summarized in Table 3.1. The implicit method provides a choice of implicit operators for the integration purpose whereas the explicit method uses the central-difference operator. The implicit method is unconditionally stable, whereas the explicit method which uses central difference integration rule is only conditionally stable when the time increment is small. The use of small increments is advantageous because it allows the solution to proceed without iterations and without requiring tangent stiffness matrices to be formed. It also simplifies the treatment of contact. Changes in contact are extremely non-linear. Because of this, and implicit algorithm typically needs many iterations to resolve it. This is computationally expensive. Challenging contact problems are therefore often solved more easily in explicit method.

In an implicit dynamic analysis, the integration operator matrix must be inverted, and a set of nonlinear equilibrium equations must be solved at each time increment. However, in an explicit dynamic analysis, displacements and velocities are calculated in terms of quantities that are known at the beginning of an increment. Therefore, the global mass and stiffness matrices need not be formed and inverted, which means that each increment

is relatively computational inexpensive compared to the increments in an implicit integration scheme. Thus, explicit method was chosen as it is more favorable and computationally efficient in this study.

Table 3.1: Key differences between implicit and explicit

	Implicit	Explicit
Problems	Low speed non-linear dynamic	High speed dynamics
Material models	Wide range of material models	Includes failure material models
Contact formulation	Basic contact problems	Complex contact problems
Solution technique	Unconditionally stable	Conditionally stable
Disk space and memory	Large	Smaller

3.3 Mass scaling method

In the explicit method, mass scaling method were used in the simulation study to speed up the simulation time. It enables to control the stable time increment to obtain a quasi-static solution with less computational time. In a general rule of thumb for simulation results to be acceptable, kinetic energy typically falls between the range of 5-10% of internal energy.

$$\Delta t = \frac{L_{min}}{c_d}$$

3.4 Relationship of line speed

The scope of this study is to investigate the effect of line speeds of 1, 10, 100 and 1000 m/min (mpm) on the degree of coil break formation. However, in order to configure the line speed in Abaqus/CAE, a parameter was required to relate the relationship with the line speed. Thus, the following formula was used:

$$v = \pi DN$$

Where:

v = line speed (mm/min)

D = diameter of coil (600 mm)

N = rotational speed of uncoiler (rev/min)

Since rotational speed of uncoiler, N is directly proportional to the line speed. The N value shown in Table 3.2 was configured and used to investigate the relationship between the line speeds and coil break formation.

Table 3.2: Relationship between line speed and rotational speed of uncoiler

V (m/min)	V (mm/min)	N (rad/s)
1	1000	0.0556
10	10000	0.5556
100	100000	5.5556
1000	1000000	55.5556

3.5 Model setup

The 3D simulation model based on the explicit analysis were successfully developed to simulate the uncoiling process. Each of the modules and its settings were explained in detail in their respective section. The rest of the settings were set as default.

3.5.1 Part Module

3.5.1.1 Uncoiler Design

The uncoiler design is divided into four quadrants. Each quadrant of the uncoiler has a radius of 300 mm whereby the total diameters of the 4 segments uncoiler are 600 mm with a width of 360 mm as shown in Figure 3.2. The uncoiler is modelled as an analytical shell element as the study only focused on the deformation of the LCS sheet. Inertia point mass of 1 were assigned for the uncoiler in the simulation model.

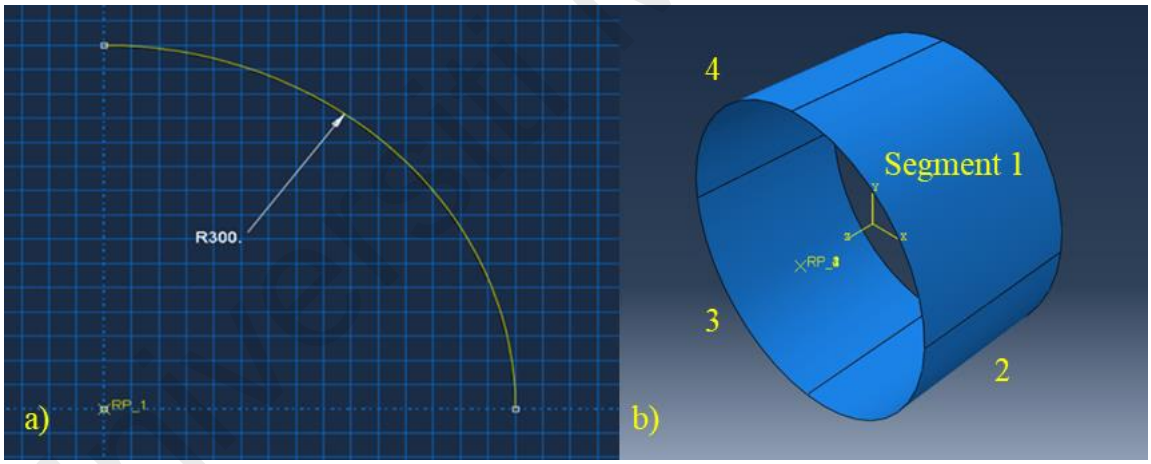

Figure 3.2: Uncoiler design (a) 2D dimensions (b) 3D model view

3.5.1.2 Coil sheet Design

Coil sheet metal in this FE simulation were modelled as a deformable shell. There are approximately only two coil laps are constructed around the inner core diameter of 600 mm with a width of 300 mm as shown in Figure 3.3. The left side of the coil sheet is constructed from the point origin while the right side has a 0.75 mm vertical offset. The thickness of coil sheet with 0.75 mm were assigned on top and below the shell elements.

The remaining laps in the coil were not included for reduction of simulation and computational cost.

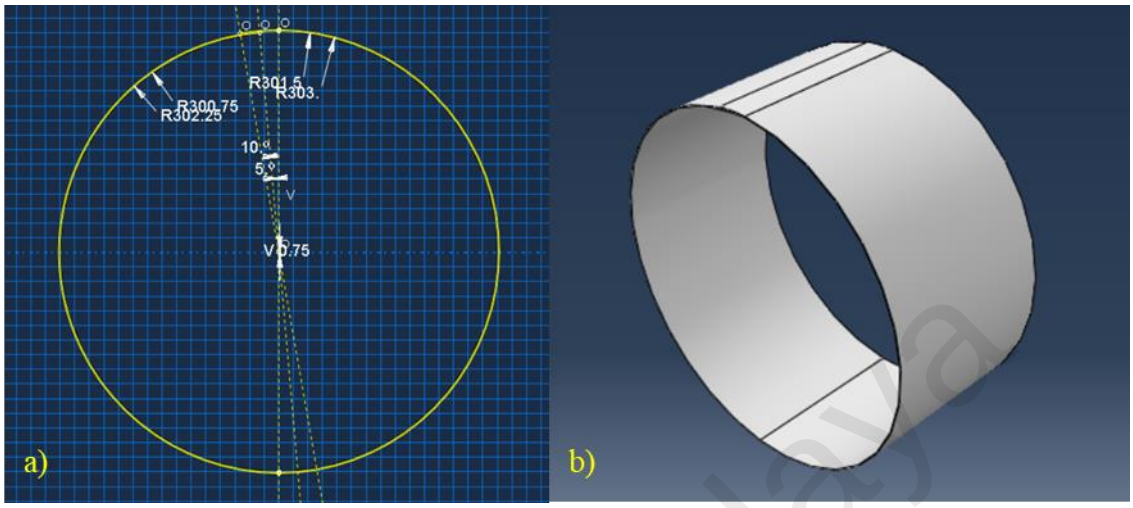

Figure 3.3: LCS coil sheet (a) 2D dimensions (b) 3D model view

3.5.2 Property Module

3.5.2.1 Low Carbon Steel

Table 3.3 and 3.4 shows the chemical and mechanical properties of fully annealed low carbon steel sheet used in the simulation settings. The tensile properties of the low carbon steel samples (size 13B) with JIS Z 2241 standard were obtained by using universal testing machine as shown in Figure 3.4. During testing, the load and displacement values are recorded from the machine to a chart recorder. The true stress-strain curve of the coil ends was used to define the material properties as more coil breaks are found near the coil ends. Thus, 3 stress-strain curves under different strain rate of the coil ends were obtained with a crosshead speed of 600, 350 and 20 mm/min respectively as shown in Figure 3.5.

Figure 3.4: Tensile specimen of LCS sheet

Table 3.3: Chemical properties of LCS sheet

Carbon	Silicon	Manganese	Phosphorus	Sulphur
0.04	0.02	0.15	0.012	0.009

Table 3.4: Mechanical properties of LCS sheet

Mechanical Properties	Value
Mass Density	7850 kg/m3
Young Modulus	206000 MPa
Poisson's ratio	0.3

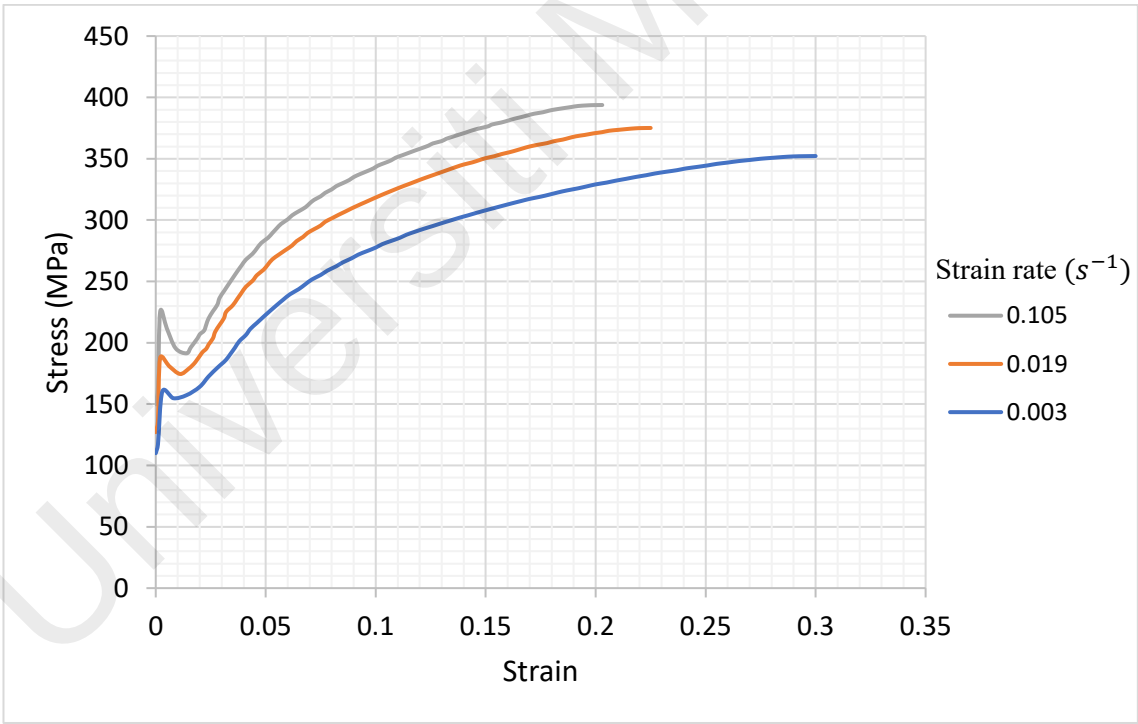

Figure 3.5: Stress strain curve of low carbon steel at different strain rate

3.5.3 Assembly and Interaction Module

The uncoiler and LCS coil sheet were assembled with the datum center point as reference point in Figure 3.6. Friction is an important parameter in real life condition. However, it is often not considered in specific detail in metal sheet simulations based on past researcher studies. The current industrial standard is to use a constant coulomb coefficient of friction which limits the overall simulation accuracy. Thus, a standardized penalty contact friction of 0.5 were defined for the 2 sets of dry contacting surfaces in the Abaqus as shown in Table 3.5.

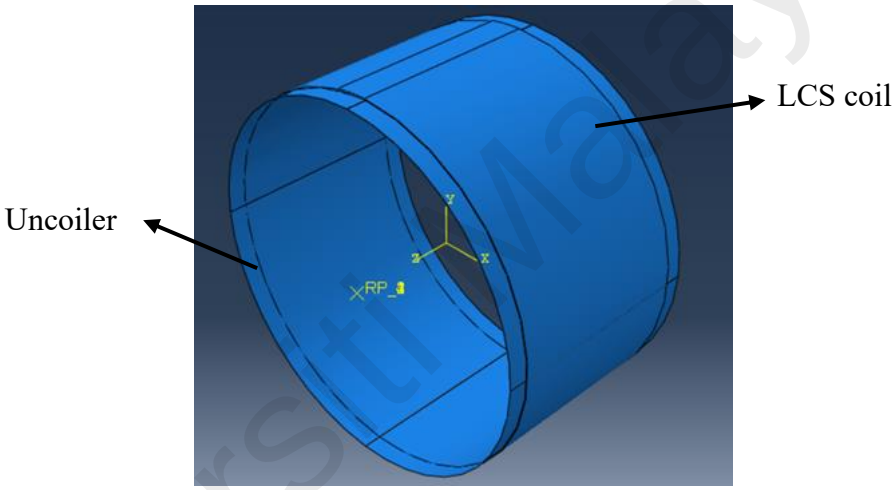

Figure 3.6: Assembly part module

Table 3.5: Interaction module settings

Surface contact	Coefficient of friction
Uncoiler and bottom surface of LCS sheet	0.5
Self-contact of LCS coil sheet	0.5

3.5.4 Step Module

There are a total of 6 steps to simulate the uncoiling process as shown in Table 3.6. The initial step was to define the initial conditions of the uncoiler. Then, each quadrant of the uncoiler were expended 0.1 mm outward to obtain a firm contact between the surfaces before uncoiling. Edge loads such as forward and backward tensions were applied to flatten the LCS coil sheet during uncoiling in Step 3. The uncoiling process begins when it starts to uncoil with a rotational speed of 0.0556 rad/s for the first and 2nd round in Steps 4 and 5 respectively. Lastly, the uncoiler then proceeds to uncoil the remaining laps of the LCS sheet.

Table 3.6: Step module settings for 1mpm

Steps	Explanation	Time (s)	Rotational speed of uncoiler (rad/s)
1	Set initial conditions of uncoiler	-	-
2	Expand uncoiler 0.1 mm outward	1	-
3	Apply forward and backward loads	1	-
4	Uncoil 360	113.0069	0.0556
5	Uncoil 360 to 720	113.0069	0.0556
6	Uncoil 720 to remaining lap	3.1390	0.0556

3.5.5 Load Module

Boundary conditions were defined to prevent any unnecessary motion of the model. In the initial step, 6 degrees of freedom of the coil front, coil end and coil edges are fully constrained to prevent any movement. When the uncoiler begins to uncoil in Step 4, rotation movement of the model about the y-axis and the displacement along the x-axis are constrained, whereas the others are set free.

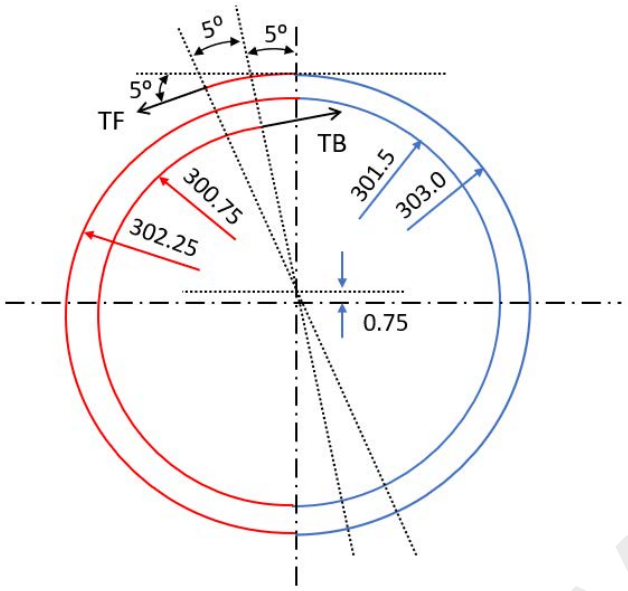

Figure 3.7: Load assigned to the coil sheet

Forward tension line load, *TF* at an angle of 5˚ from the horizontal axis ranging from 36 to 176 N/mm were applied along the longitudinal direction to flatten the coil. Conversely, a pairing load of backward tension, *TB* with a magnitude of the 35 to 175 N/mm were also applied in the direction towards the coil end as shown in Figure 3.7. The magnitude of the coiling tension was varied to minimize the coil break formation. The magnitude of backward tension, *TB* was assigned in such a way so that the coil sheet does not slide over the uncoiler during the simulating process. Loads that were assigned to the 3D simulation model were summarized in Table 3.7.

Table 3.7: Loads module settings

Load	Value
Forward Tension, TF	36 to 176 N/mm
Backward Tension, TB	35 to 175 N/mm
Gravity	9.81 m/s2

3.5.6 Mesh Module

The LCS coil sheet were meshed using S4R 3D shell element which have 4-node general purpose shell, reduced integration with hourglass control and finite membrane strains. S4R 3D shell element was chosen because of their ability to act as both thin and thick shells and can be used for general finite strain applications. A global seed size of 18 mm with 10 shell elements were assigned in the coil sheet. The completed and verified mesh formation can be seen in Figure 3.8. The number of integration points of 3, 5 and 7 were also varied in the thickness direction to determine the effect on simulation accuracy and computational time. The mesh module settings were summarized in Table 3.8.

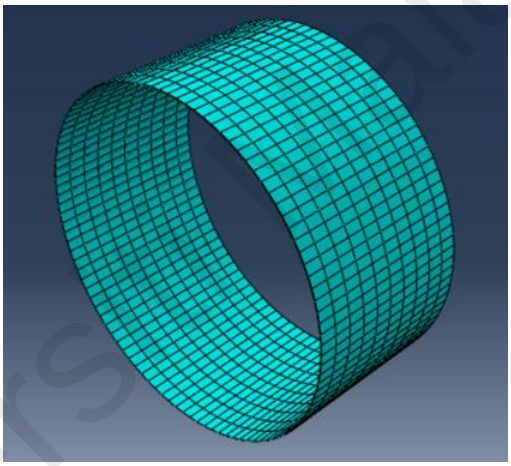

Figure 3.8: Mesh module of LCS coil sheet

Table 3.8: Mesh module settings

Parameters	Value
Shell elements	S4R
Integration points	3, 5 and 7
Global seed size (mm)	18

CHAPTER 4: RESULTS AND DISCUSSION

4.1 Simulation results

The simulation results were obtained with 10th Generation Intel® Core™ i7-10875H Processor (Eight Core, Sixteen Threads, 2.3GHz to 5.1GHz), 16M Cache and a memory of 16GB RAM. Abaqus/Explicit analysis with single precision were used in the simulation settings. The true strain values were calculated based on 3 Simpsons integration points across the shell thickness of 1.5 mm. The coil tension is fixed at 166 N/mm to investigate the effect of line speed. All the simulation results except 1 mpm line speed were obtained with a sampling rate of 0.0002s with no mass scaling. However, there is a limitation in the study whereby the 1 mpm line speed which completed until 1 lap required about 16 hours and it was not feasible as it was estimated that the total computational time will require more than 32 hours. Thus, the simulation results of 1 mpm were mass scaled to a mass density of 78500 kg/m3 (ratio of 10) with a sampling rate of 0.01s due to the limitation of large file size data with a computational time more than 24 hours. Mass scaling (MS) was used in the 1 mpm simulation settings to increase the stable time increment for faster computational time by increasing the mass density. Hence, the total computational time of 1 mpm with mass scaled were able to be completed within 12 hours. In addition, mass scaling can only be done within a ratio of 10 as any ratio more than it will cause an excessive mass scaling with erroneous results. The comparisons of the LE11 strain distributions along the front and mid path of the uncoiled sheet between the mass scaled and the first lap completion of the original mass of 1 mpm were shown in Figure 4.1 and Figure 4.2. The simulation results of 1 mpm with mass scaled were valid and used in the results analysis as it was observed that the first lap of the LE11 strain distributions of the mass scaled were similar to original mass of 1mpm. The total computational time of increasing line speed were shown in Figure 4.3. The computational time of 1 mpm line speed takes the longest as its time period is the largest.

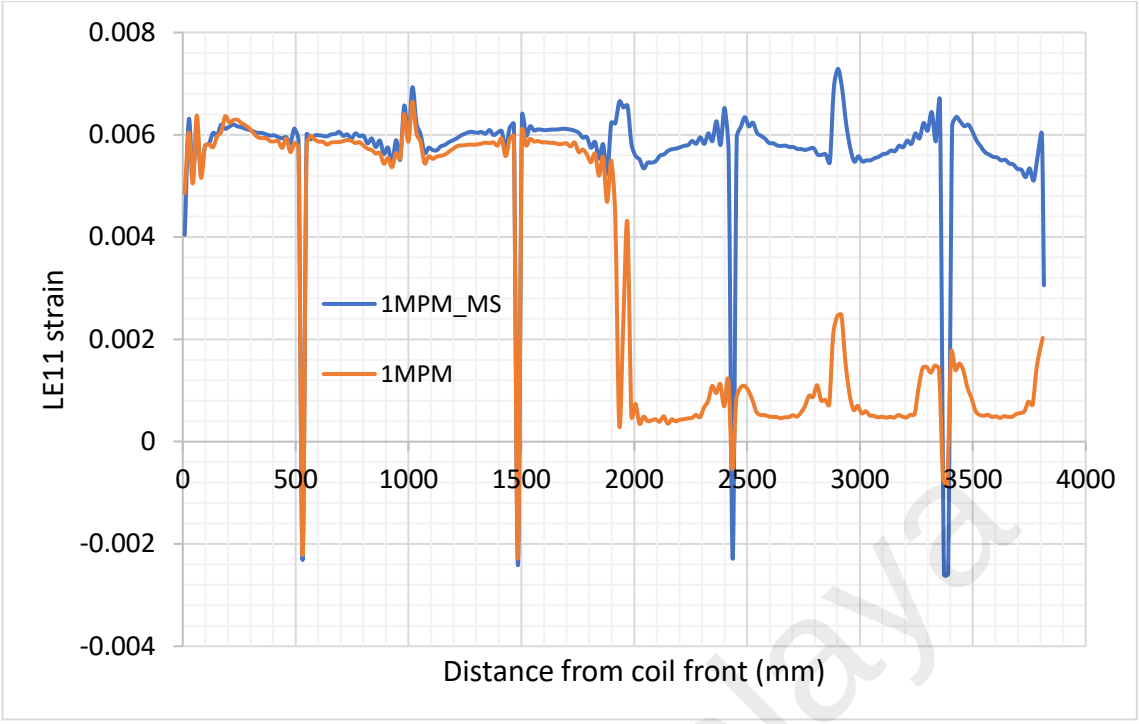

Figure 4.1: Comparisons of true LE11 strain distributions along the front path of uncoiled sheet at 1mpm between mass scaled and original mass.

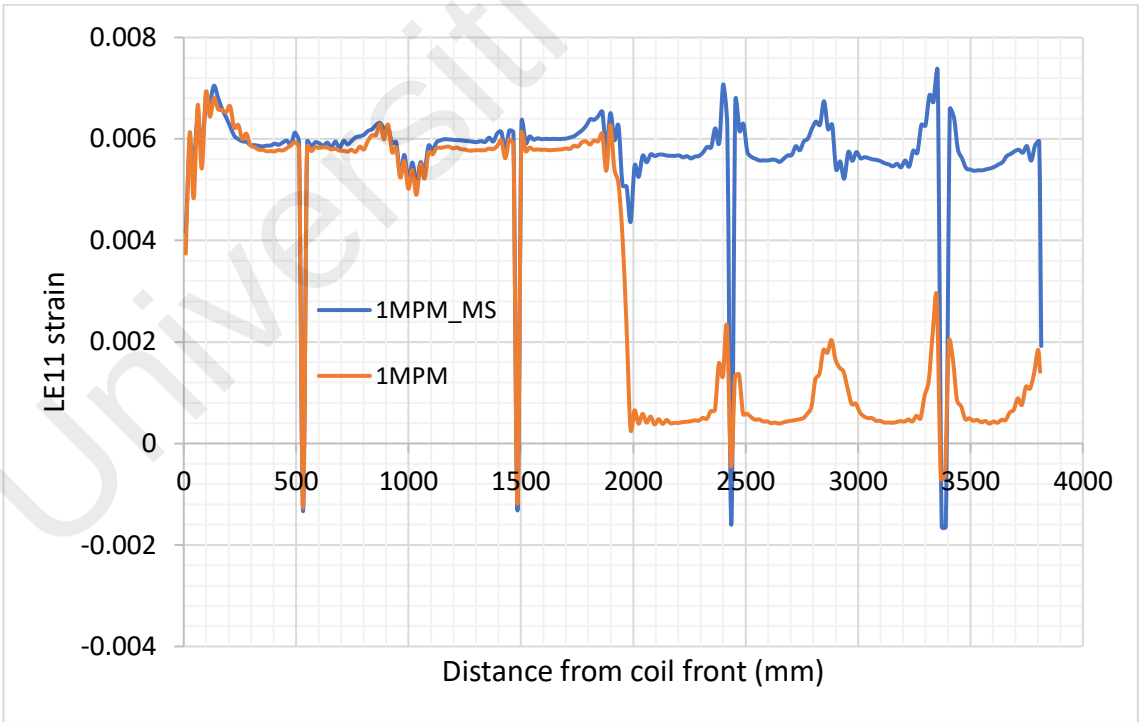

Figure 4.2: Comparisons of true LE11 strain distributions along the middle path of uncoiled sheet at 1mpm between mass scaled and original mass.

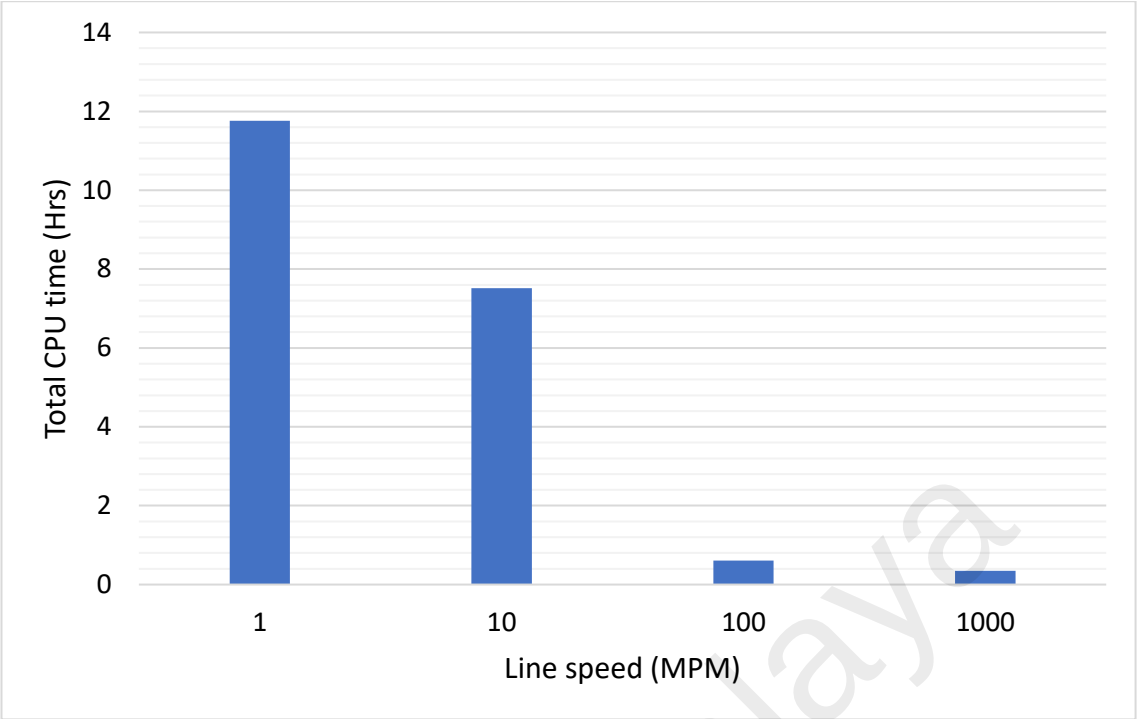

Figure 4.3: Total computational time of increasing line speed with coil tension of 166 N/mm

4.2 Effect of forming speed

The effect of forming speed on coil breaks were investigated with the coil tensions fixed at 166N. It can be observed that there a total of 7 similar patterns of interrupted strain zones (localized plastic deformation) on the top surface of uncoiled sheet as shown in Figure 4.4 and Figure 4.5. The localized plastic deformation zones were characterized into 4 zones A and 3 zones B. The uninterrupted strain zones values decreased with an increase of line speed from 1 to 1000 mpm as seen in Figure 4.4. This can be explained due to the stretching of the 2 lap coil sheets at a faster rate in higher line speed. Based on Figure 4.4, Zones A have narrow bands with LE11 strain distributions of compressive (negative) value whereas Zone B have islands of tensile (positive) value. Zone B have islands of tensile strain value lower than the uninterrupted zone in the middle path. Thus, the strain distributions of zone B are uneven as the strain values of front path are higher than the middle path. The islands of tensile strain in Zone B were due to the incomplete bending which leads to the formation of coil break. In comparison, Zone A have a more

uniform LE11 strain distributions across the top surface of sheet at 10 to 1000 mpm. It could be seen that highly concentrated compression strains start to form at the edge portions of Zone A1 and A2 at 1 mpm in Figure 4.4 (a). The narrow bands of Zone A with highly concentrated compressive strains in the uncoiled sheet surface are unfavorable as it could pose a risk of buckling. Therefore, it is crucial to remove all localized compressive strain on the top surface.

The localized plastic deformation in Zone A leads to the high concentration of compressive strain whereas island of tensile (positive) LE11 strain leads to the coil break formation in Zone B. The distances between the interruption zones were similar and repeated in the distribution for all line speeds.

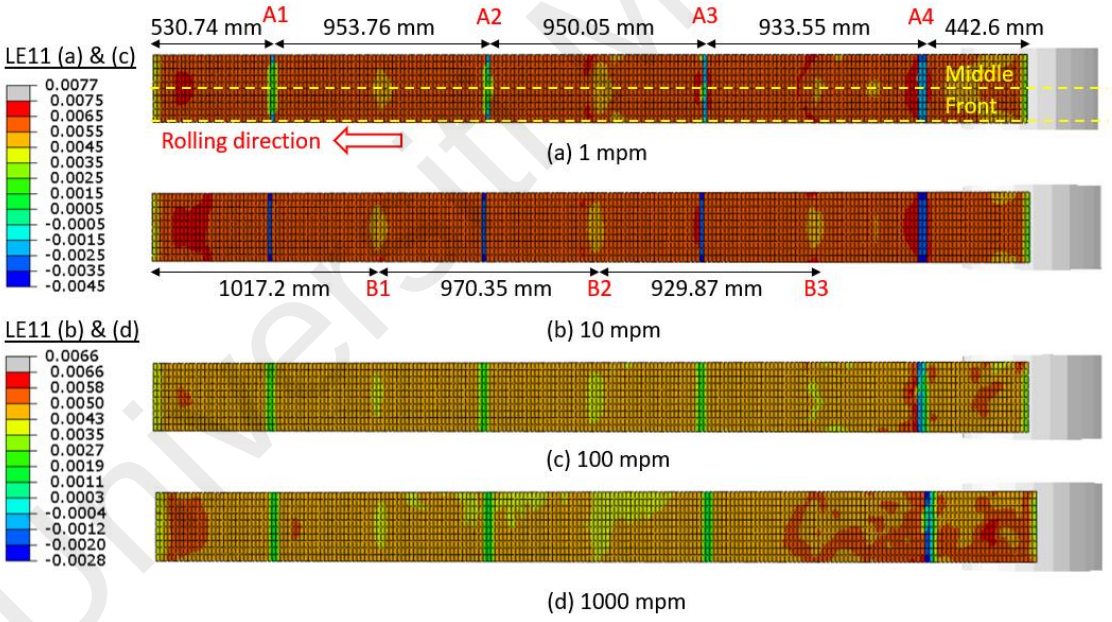

Figure 4.4: True LE11 strain distributions along the top surface of uncoiled sheet at different line speeds.

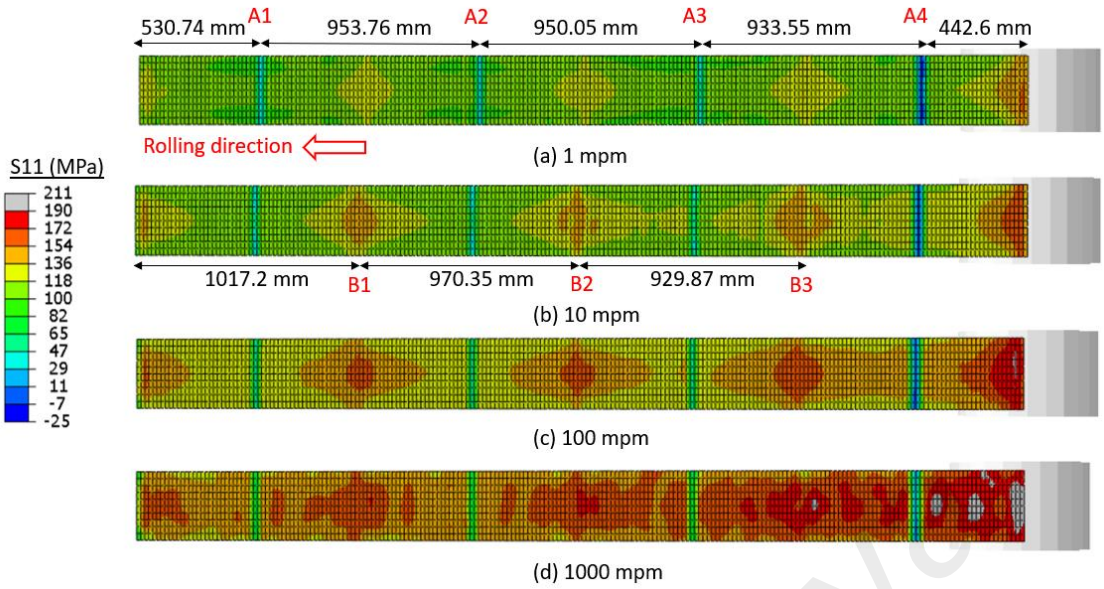

Figure 4.5: S11 stress distributions along the top surface of uncoiled sheet at different line speeds.

The S11 stress distributions on the top surface of the uncoiled sheet under different forming speed are shown in Figure 4.5. It was observed that the interrupted zones of S11 stress distributions in Figure 4.5 are similar with the interrupted zones of LE11 strain distributions as shown in Figure. 4.4. Particularly, same amount of similar Zones A and B were obtained. The Zones A have narrow bands with highly concentrated S11 stress distributions of compressive (negative) value whereas Zone B have islands of tensile (positive) value. The S11 stress distribution values in the uninterrupted zones increased which leads to a reduction of compressive stress values in Zone A. In addition, the concentration area and S11 stress distribution values of Zone B becomes bigger with increase of line speed. The magnitude of the compressive stress was able to decrease by increasing the line speed. According to Tan and Liew (2021), the uncoiled sheet tends to retain its original curvature shape under the compressive stress without the coil tension. Therefore, the effect of coil tensions shall be further carried out to investigate the optimum coil tensions with the optimum line speed to minimize both the highly concentrated compressive strain and coil break.

The LE11 strain distributions along the front paths on the top surfaces of the uncoiled sheets with increasing line speed are shown in Figure 4.6. In general, the LE11 strain levels of the uninterrupted zones decreased with increasing line speed. It could also be observed that the valley and peaks of Zone A and B decreased with increasing line speeds. Furthermore, a sudden spike height of strain value was observed at an uncoiled length near the coil front (0-225 mm) and coil end (3000-3810 mm). This can be explained due to the forward and backward tensions were applied instantaneously at the coil front and coil end in the simulation settings. However, this situation does not occur in the industry as the tensions were applied gradually in the manufacturing line. Thus, the results of Zone A4 were excluded and only results from Zone A1, A2 and A3 and Zones B were considered in results analysis.

The LE11 strain distributions along the middle paths on the top surfaces of the uncoiled sheets with increasing line speed were shown in Figure 4.7. The LE11 strain values in Zone A are negative (compressive) whereas the ones in Zone B are positive (tensile). It was observed clearly that there is no significant change on the maximum peak of zone A at increasing line speed as shown in Figure 4.6 and Figure 4.7. However, the uninterrupted zone was significantly reduced in comparison at higher line speed. Hence, the optimum speed could be obtained at higher line speed as the reduction of LE11 strain in the uninterrupted zone would result in a lower LE11 peak height in Zone A. In comparison to the front paths, valley heights of LE11 strain values for Zone B in the middle path are found to have a sudden spike drop. This can be explained due to the incomplete unbending of the uncoiled sheet at Zone B. Overall, the LE11 strain distributions in the uninterrupted zone decrease with an increase of line speed. However, no formations of coil break or localized tensile strain would be resulted from these highly LE11 compressive strain in zone A as a results of increasing line speed.

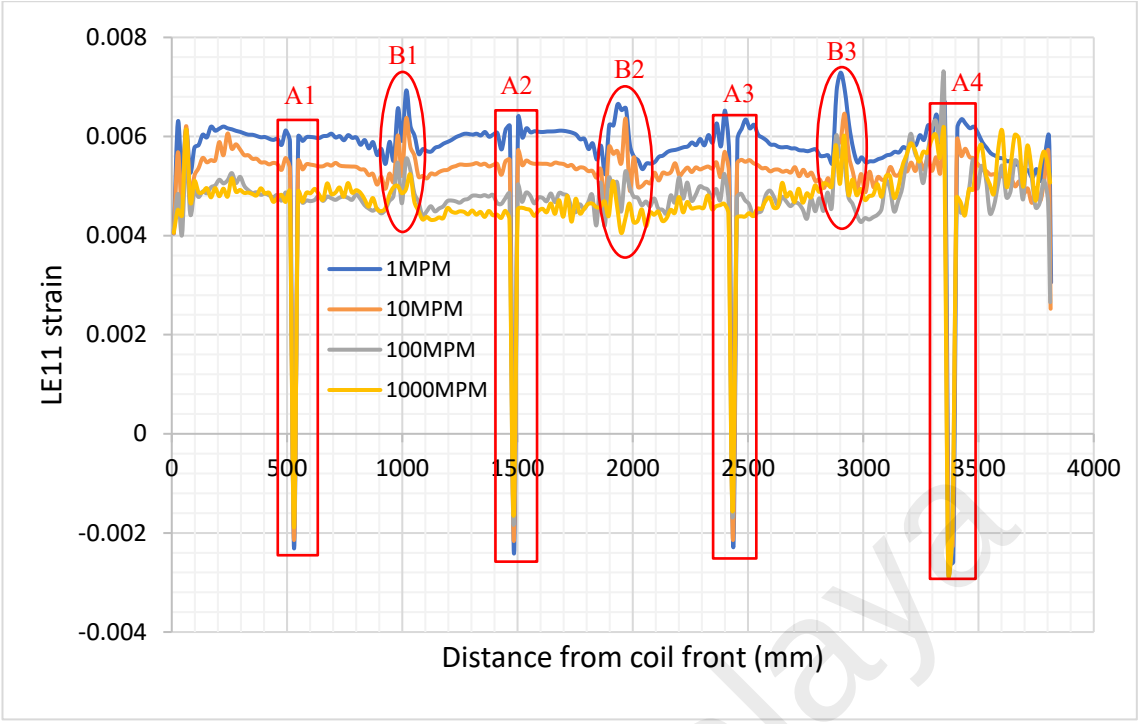

Figure 4.6: LE11 strain distributions along front path on top surface of uncoiled sheet at different line speeds.

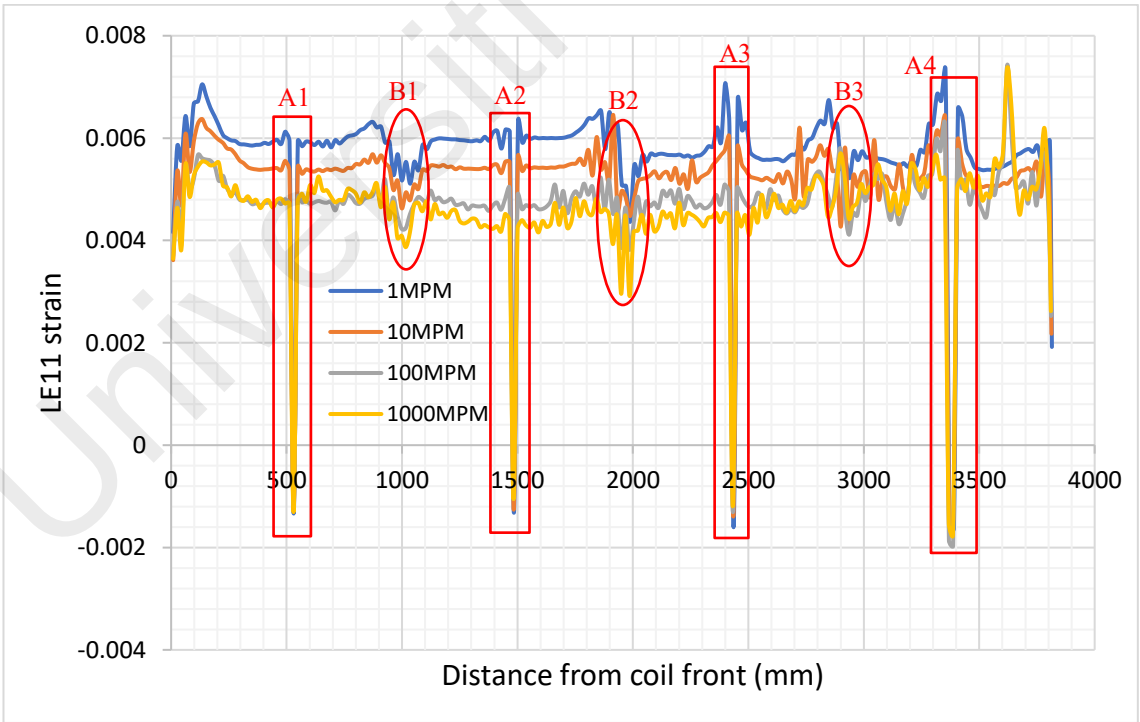

Figure 4.7: LE11 strain distributions along middle path on top surface of uncoiled sheet at different line speeds.

The relative peak and valley heights in Zone A and Zone B under different line speeds were summarized in Figure 4.8. The absolute average LE11 strain values were then determined and plotted. The minimum absolute average LE11 strain value of 0.00365 were obtained at forming speed of 1000 mpm. It was observed that the overall trend of coil break or tensile strain in Zone B is decreasing with the increased of line speed. However, the amount of change in the compressive strain in Zone A is more significant at higher line speed. Moreover, the LE11 strain value decreased in the front path of Zone B from 1 to 1000 mpm. However, an adverse effect is found at 1000 mpm where there is a slight increase in the middle path of Zone B. Hence, minimum coil break (positive LE11 strain) could be obtained with 100 mpm but with higher concentrated compressive strain. The decrease of LE11 in the front path may be due to the forming speed is too fast for the coil tensions to straighten out the coil sheet. In general, the absolute average LE11 peak height decrease with the increase of line speeds. Thus, 1000 mpm were chosen as the optimum line speed as it has the lowest absolute average LE11 strain.

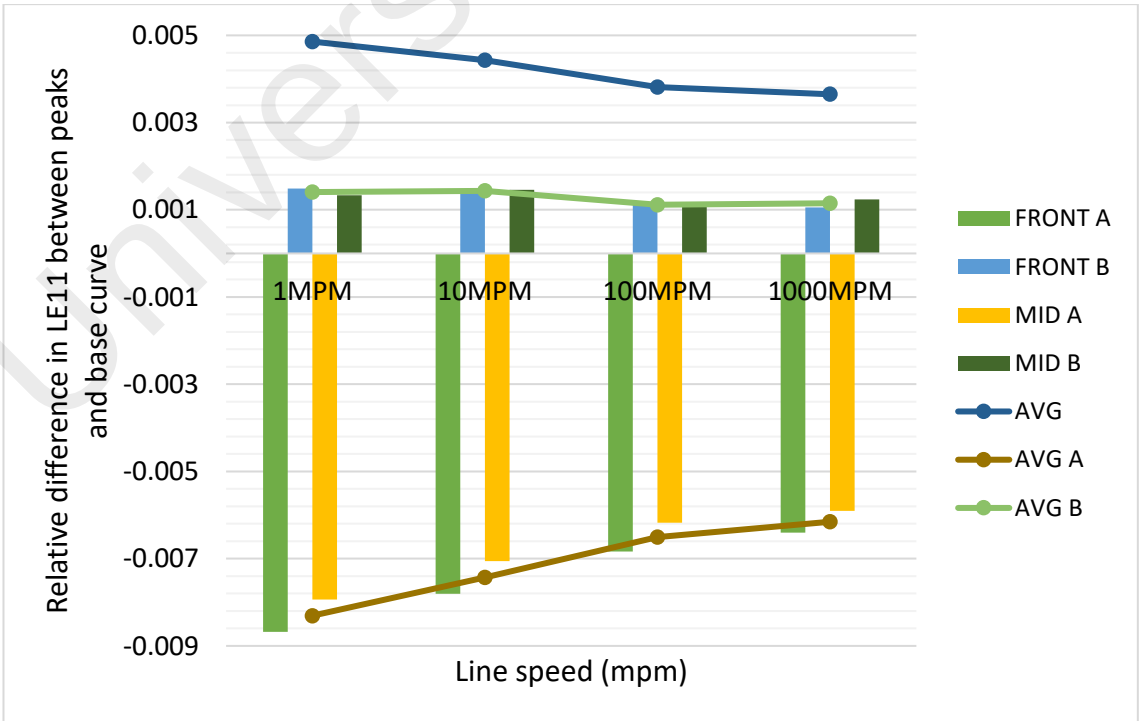

Figure 4.8: Relative difference in LE11 between peaks and base curve on top surface of uncoiled sheets at different line speeds

The LE11 evolution of front and middle elements in Zone A1 and B1 were investigated to determine the strain rate during the tangent point as shown in Figure 4.9 and Figure 4.10. Since the LE11 value of uninterrupted zone is stable and uniform across the width of sheet, the middle element 1275 at the right of Zone A2 were then used as a benchmark to compare the strain rates of Zone A1 and B1 as seen in Figure 4.11. The LE11 strain distributions of Zone A1, B1 and uninterrupted zone were plotted as seen in Figure 4.12 to Figure 4.16.

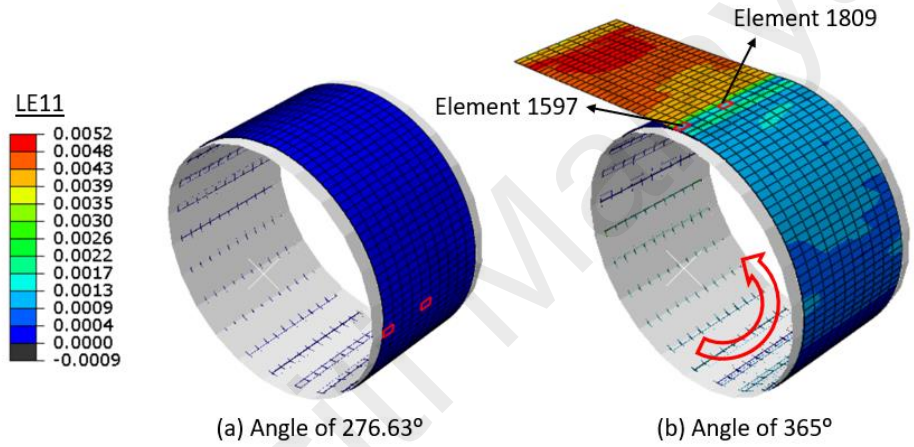

Figure 4.9: LE11 strain distributions of Zone A1 with element 1597 and 1809 at (a) Angle of 276.63 ° (b) Angle of 365 °

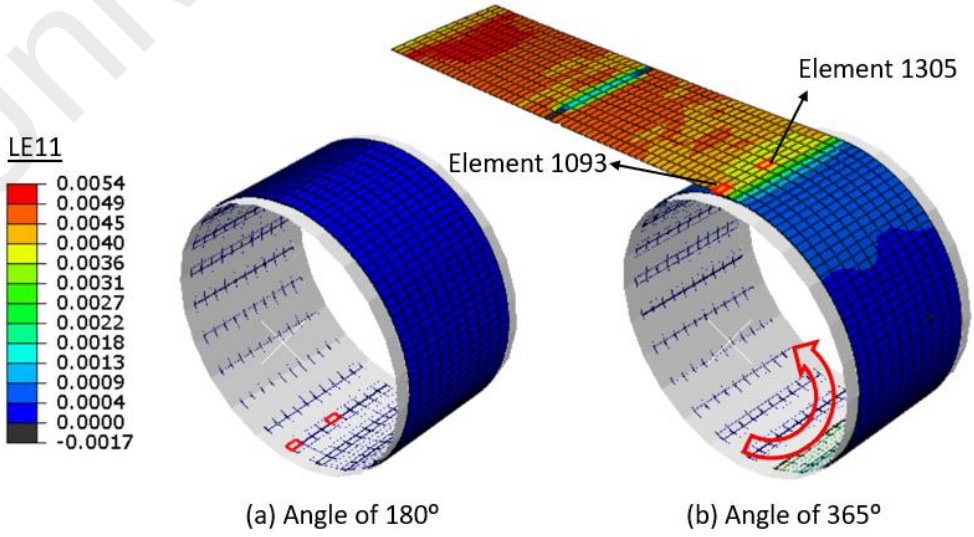

Figure 4.10: LE11 strain distributions of Zone B1 with element 1093 and 1305 at (a) Angle of 180 ° (b) Angle of 365 °

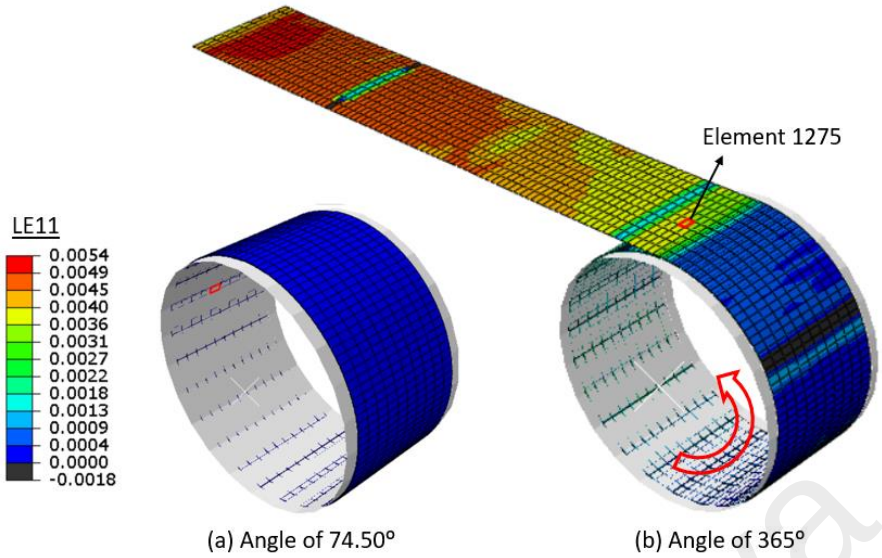

Figure 4.11: LE11 strain distributions of uninterrupted zone with middle element 1275 at (a) Angle of 74.50 ° (b) Angle of 365 °

Although noise signal was present at the highest line speed of 1000 mpm, it only has significant effect on the results of Zone A1 middle element of 1809 after the tangent point as shown in Figure 4.13. The results of Zone A1 middle element of 1809 are valid as strain rate at the tangent point has minimal noise signal distributions. The strain of the elements in Zone A1, Zone B1 and the uninterrupted zone was observed to have a sudden spike as the uncoiler rotates about 365° as shown in Figure 4.12 to Figure 4.16. This is due to the deformation mostly takes place at the angle of 365° as the forward tension load were applied on the tangent point of 5°. However, the amount of strain rate increases around the tangent point depending on the uncoiling speed and zones of deformation as seen in Figure 4.12 to Figure 4.16. Based on Figure 4.12 to Figure 4.16, the slope during the tangent point were found to be decreasing with increasing of line speed with x-axis set as rotational angle. Under high line speed, the increase in the rotational speed is much higher than the slight decrease in LE11 slope of 1000 mpm when compared to 1 mpm. Therefore, the slope of tangent point is found to be decreasing with an increase of line speed.

A straight line was plotted against the sudden spike to determine the strain rate. For the strain rate in Zone A1 with front and middle element of 1597 and 1809, line speed of 1000 mpm has the highest strain rate value of -0.1304 s^{-1} and -0.0396 s^{-1}, whereas 1 mpm has the lowest value of -0.0003 s^{-1} and -0.0001 s^{-1} respectively. Similarly, for the strain rate in Zone B1 with front and middle element of 1093 and 1305, line speed of 1000 mpm has the highest strain rate value of 0.7061 s^{-1} and 0.8283 s^{-1}, whereas 1 mpm has the lowest value of 0.0009 s^{-1} and 0.0002 s^{-1} respectively. However, the uninterrupted zone with middle element 1275 of 1000 mpm and 1mpm has an even higher strain rate value of 1.1920 s^{-1} and 0.0007 s^{-1} respectively. The increase in strain rate in the uninterrupted zone is the highest (from 0.0007 s^{-1} to 1.192 s^{-1}) when the uncoiling speeds are increased from 1 mpm to 1000 mpm based on Figure 4.16. Thus, a high strain rate stress strain curve would result in a lower LE11 strain based on Figure 3.5. Therefore. the LE11 strain value along the base curve for 1000 mpm is the smallest among other speeds as shown in Figure 4.6 and Figure 4.7. The strain rate obtained in the results are higher than the strain rate provided in Figure 3.5 as the coil sheet is subjected to a higher line speed more than 600 mm/min.

The increase in strain rate, $\dot{\varepsilon}$ in the element of uninterrupted zone (base curve) is a few times higher than the rest of the elements in Zone A1 and B1 of 1000 mpm. The amount of increase in strain rate at the front and middle path of compressive Zone A1 are 89 to 97% less than the ones in the uninterrupted zones for 1000 mpm respectively, resulting in the largest decrease in LE11 strain value at Zone A. Therefore, lower LE11 compressive peaks are found in Zone A for 1000 mpm as shown in Figure 4.6 and Figure 4.7. Similarly, the amount of increase of strain rate in the front and middle path of tensile Zone B1 are 30 to 40% less than the ones in the uninterrupted zones for 1000 mpm respectively, resulting in a high LE11 strain value. Hence, LE11 tensile peaks are found in Zone B. In contrast, the amount of increase in strain rate at the front and middle path

of compressive Zone A1 are 57 to 86% less than the ones in the uninterrupted zones for 1 mpm respectively, resulting in a smaller decrease in LE11 strain value. Therefore, higher LE11 compressive peaks are found in Zone A for 1 mpm as shown in Figure 4.6 and Figure 4.7. Although the amount of increase of strain rate in the middle path of tensile Zone B1 are 71% less than the ones in the uninterrupted zones for 1 mpm, which resulted in a lower LE11 strain value. However, the amount of increase of strain rate in the front path of tensile Zone B is 29% more than the ones in the uninterrupted zones for 1 mpm which cause an increase of LE11 strain value. Hence, more severe LE11 tensile peaks are found in front path of Zone B1. It should also be noted that the overall LE11 strain distribution is uneven as the LE11 strain in the front and middle element are different as shown in Figure 4.12 to Figure 4.16. Moreover, it is known that there is no significant change in the concentrated compressive strain in Zone A at higher speed as shown in Figure 4.6 and Figure 4.7. Hence, 1000 mpm is the optimum line speed with minimum coil break and concentrated compressive strain as the LE11 peak height in Zone A is the smallest due to the increase of LE11 strain reduction in the uninterrupted zone.

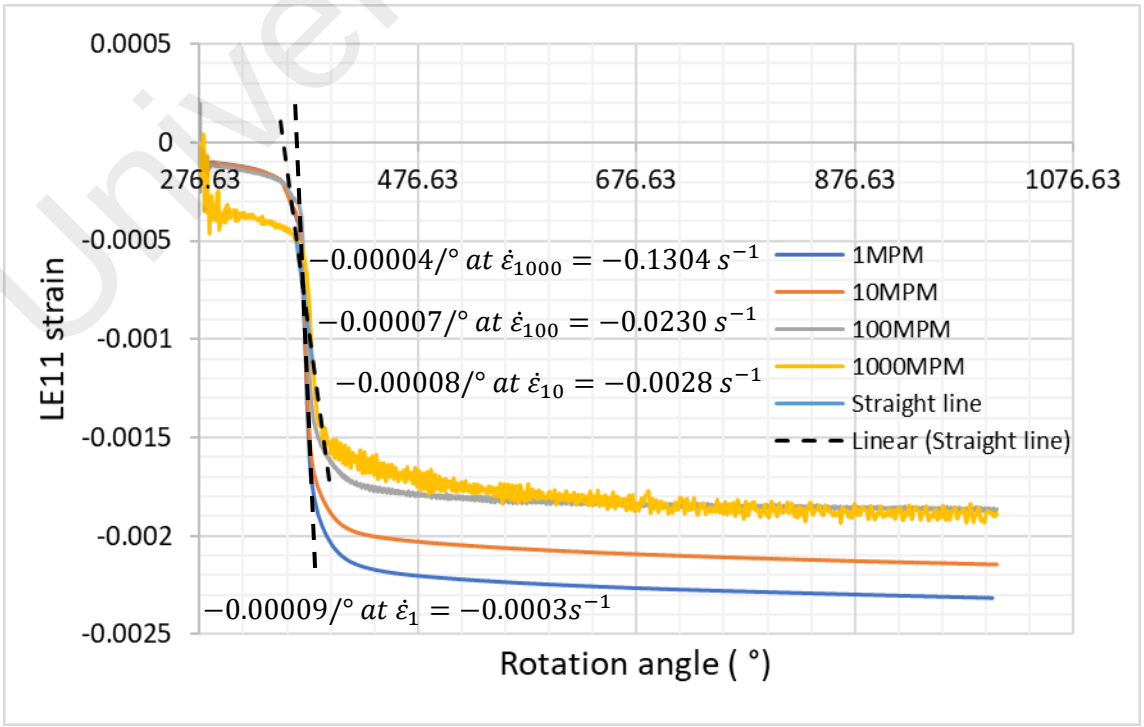

Figure 4.12: LE11 strain distributions of Zone A1 with front element 1597

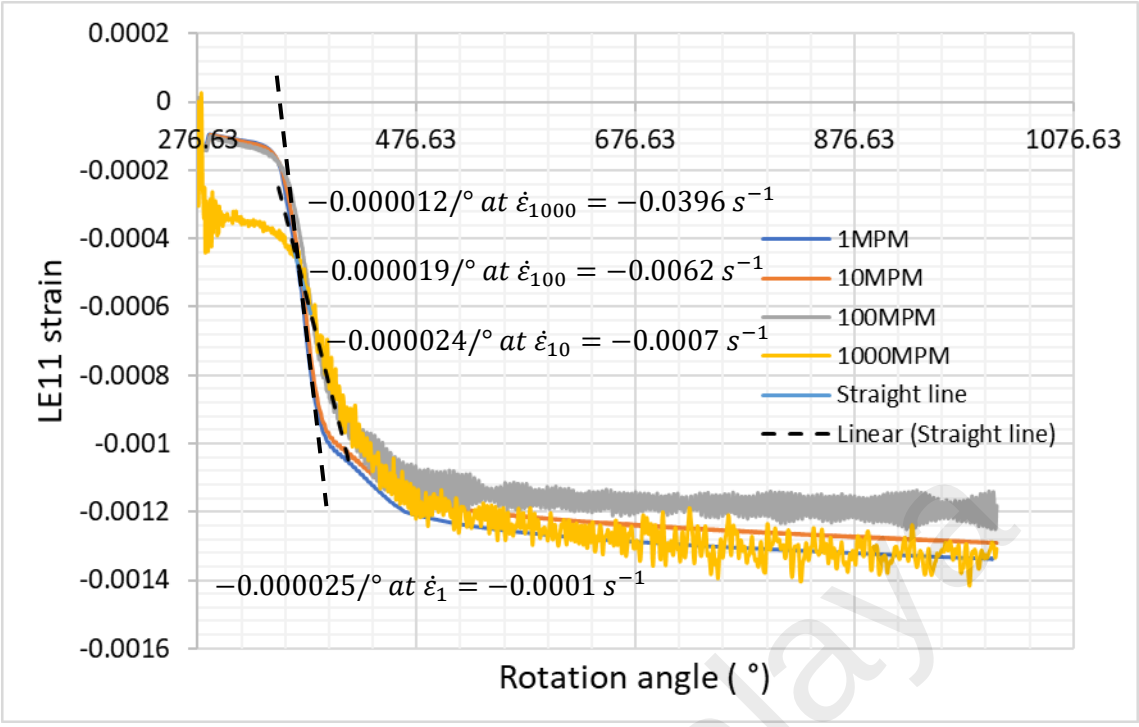

Figure 4.13: LE11 strain distributions of Zone A1 with middle element 1809

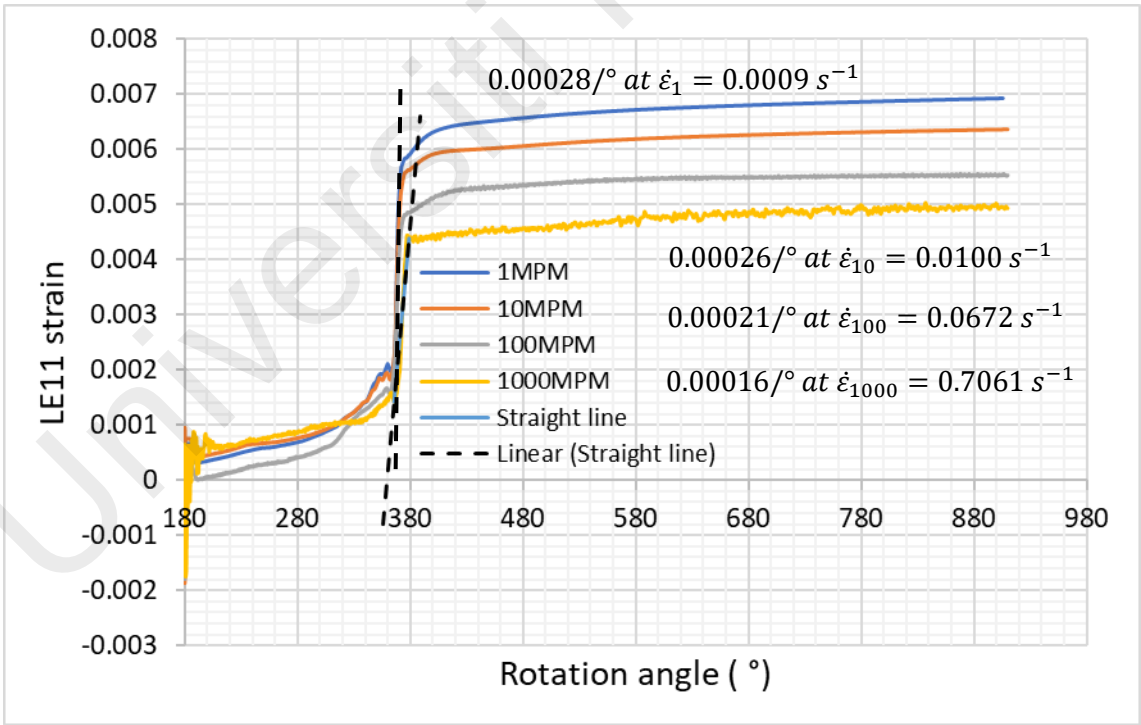

Figure 4.14: LE11 strain distributions of Zone B1 with front element 1093

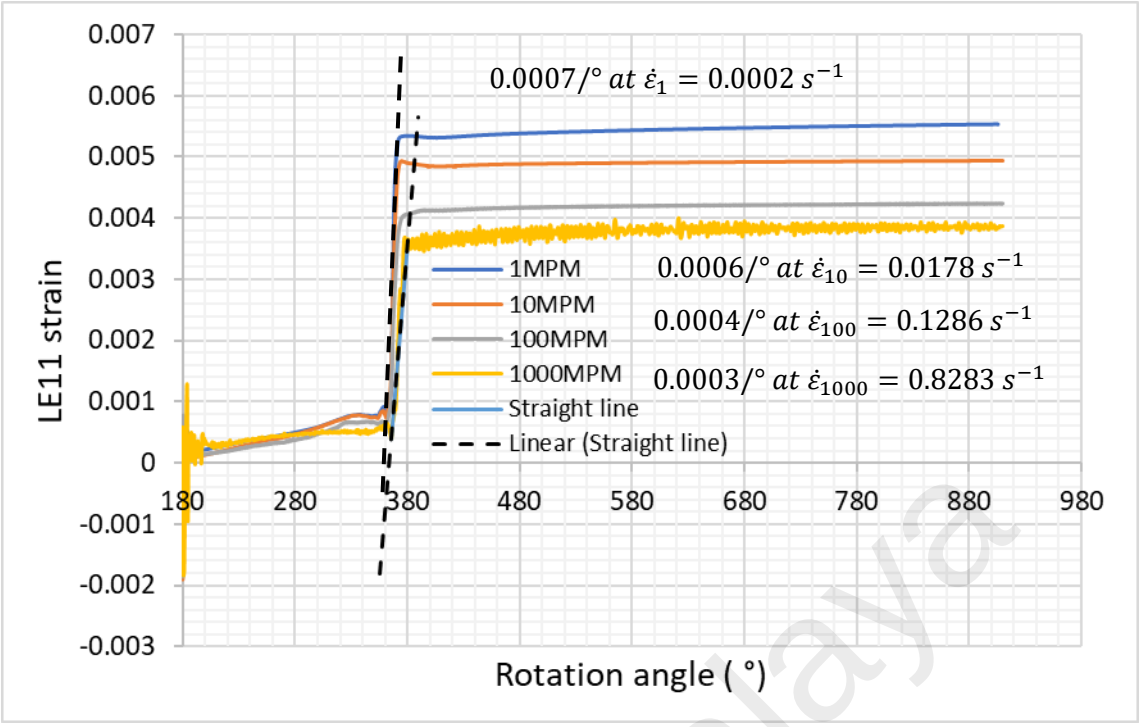

Figure 4.15: LE11 strain distributions of Zone B1 with middle element 1305

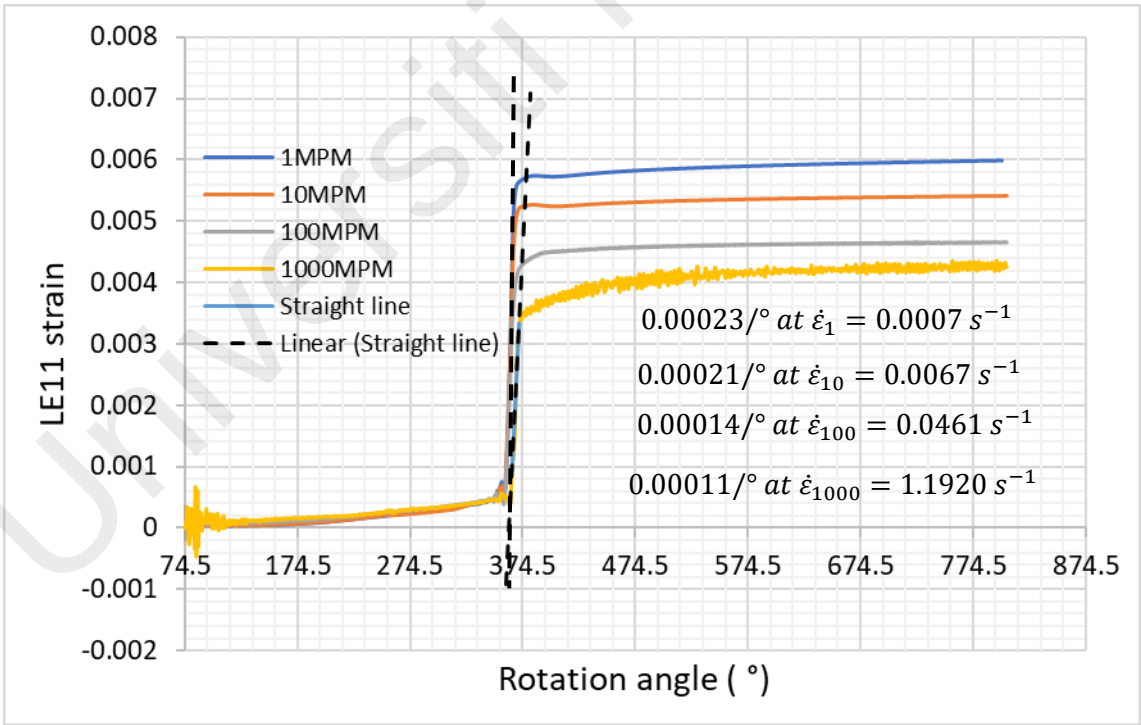

Figure 4.16: LE11 strain distributions of base curve with middle element 1275

4.3 Effect of coil tensions

The LE11 strain distributions along the front and middle paths on the top surfaces of the uncoiled sheets with increasing coil tensions are shown in Figure 4.17 and Figure 4.18. The LE11 strain values in both front and middle path at Zone A is negative (compressive) whereas the ones at Zone B are positive (tensile). It could be observed that the valley and peak of Zone A and B increased with increasing coil tensions. The increase of the high concentrated compressive strain is mainly due to a higher LE11 strain in the uninterrupted zone (base curve) with increasing coil tensions. Similarly, the results of Zone A4 were excluded and only results from Zone A1, A2 and A3 and Zones B were considered in results analysis. In comparison to the front paths, valley heights of LE11 strain values for Zone B in the middle path are found to have a sudden spike drop. The uneven island of tensile strain in Zone B were obtained due to incomplete unbending of the coil sheet. In general, the LE11 strain levels of the uninterrupted zones increased with increasing coil tensions.

The maximum peak and valley heights in Zone A and Zone B under different coil tensions were summarized in Figure 4.19. The absolute average LE11 strain values were then determined and plotted. The absolute average LE11 strain value of 0.00321 was obtained at forming speed of 1000 mpm with coil tension of 146 N/mm. Overall, a general trend was observed in Figure 4.19. It was observed that the average LE11 strain value in Zone B was decreasing to a minimum LE11 strain value at coil tension of 146 N/mm, it then rebounded and increased again at coil tension of 176 N/mm. Thus, minimum coil break could be obtained with a coil tension of 146 N/mm as the average LE11 strain value in Zone B is the lowest. Moreover, there is a significant decreased of the concentrated compressive strain in both front and middle path of Zone A with an increase of line speed. The relatively large difference of high concentrated compressive strain in Zone A with

coil tension of 146 N/mm is not a major issue as it LE11 peak value of -0.0054 is very small. Thus, the risk of buckling can be neglected.

The increased in the LE11 strain in the front path of Zone B could result into a high degree of edge coil break. Hence, a lower degree of edge breaks could be obtained with a minimum coil tension of 156 N/mm. According to Tan and Liew (2021), the increase of LE11 strain value in the front path of Zones B is mainly due to the increase of the curvature shape across the uncoiled sheet with an increase of coil tension. However, an adverse effect is found whereby higher LE11 strain were also present in the front path of Zones B at lower coil tensions. In the industries, this occurrence usually does not occur as a punch roller would be stationed in front of the uncoiler to prevent the uncoiled sheet from curling. The punch roller was not included as more computational resources are required for the simulation. In general, the absolute average LE11 peak increased with the increasing of coil tensions. By neglecting the high concentrated compressive strain, 1000 mpm with coil tension of 146 N/mm was chosen as the optimum profile to minimize the coil breaks.

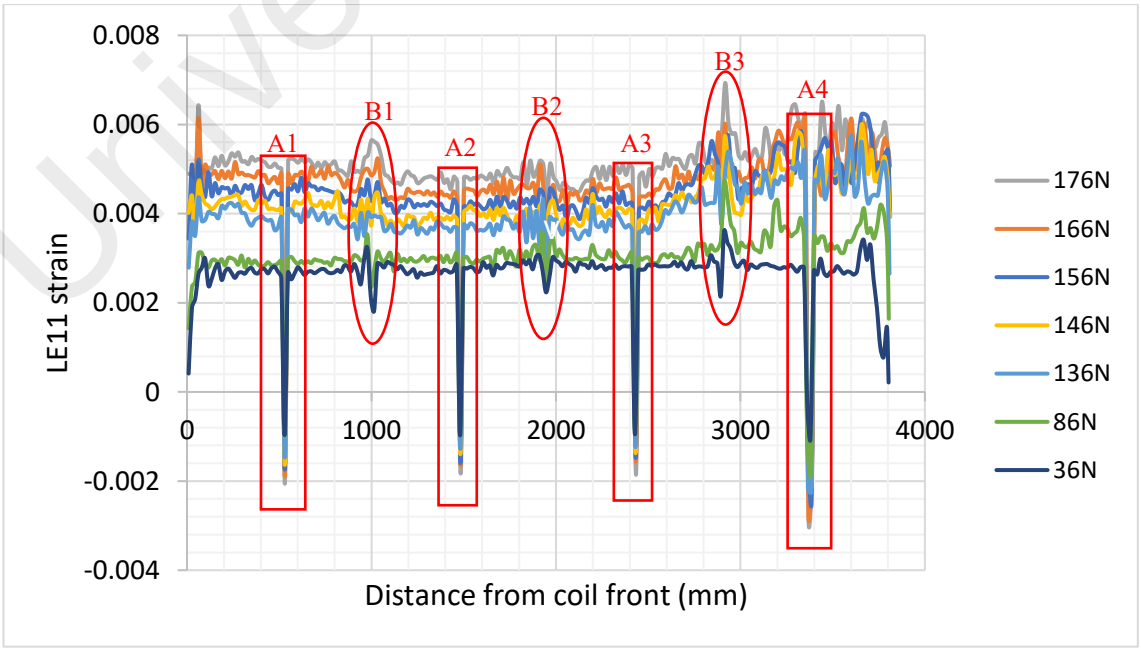

Figure 4.17: LE11 strain distributions along front path on top surface of uncoiled sheet with 1000 mpm at different coil tensions.

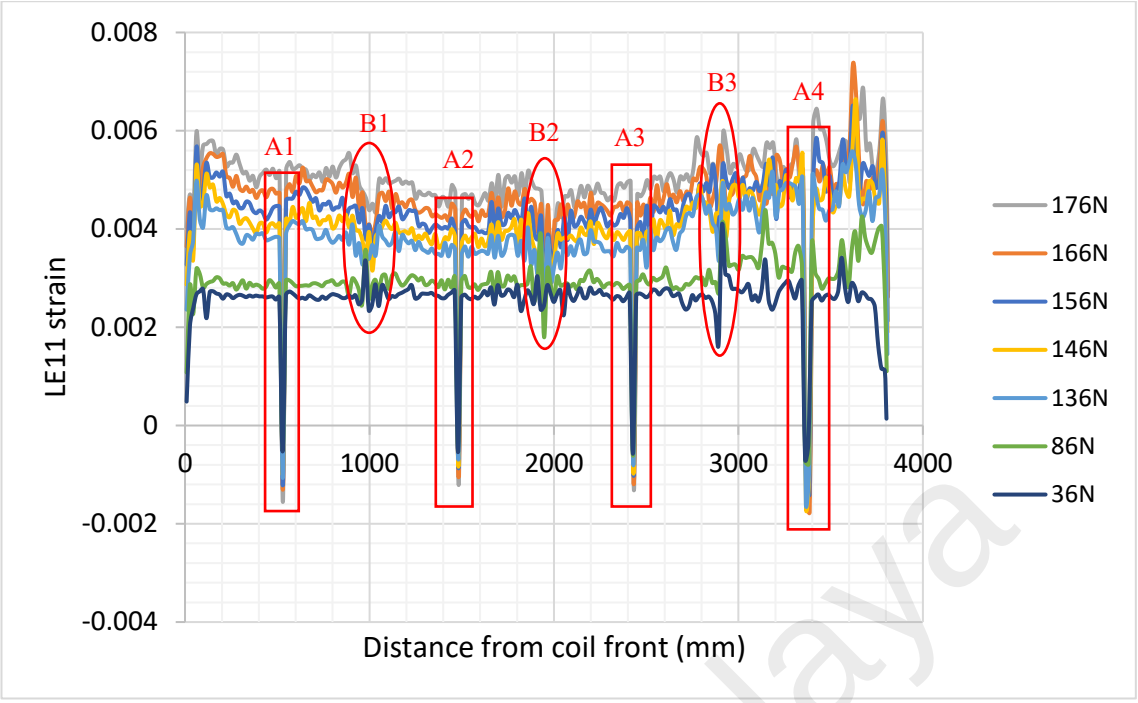

Figure 4.18: LE11 strain distributions along middle path on top surface of uncoiled sheet with 1000 mpm at different coil tensions.

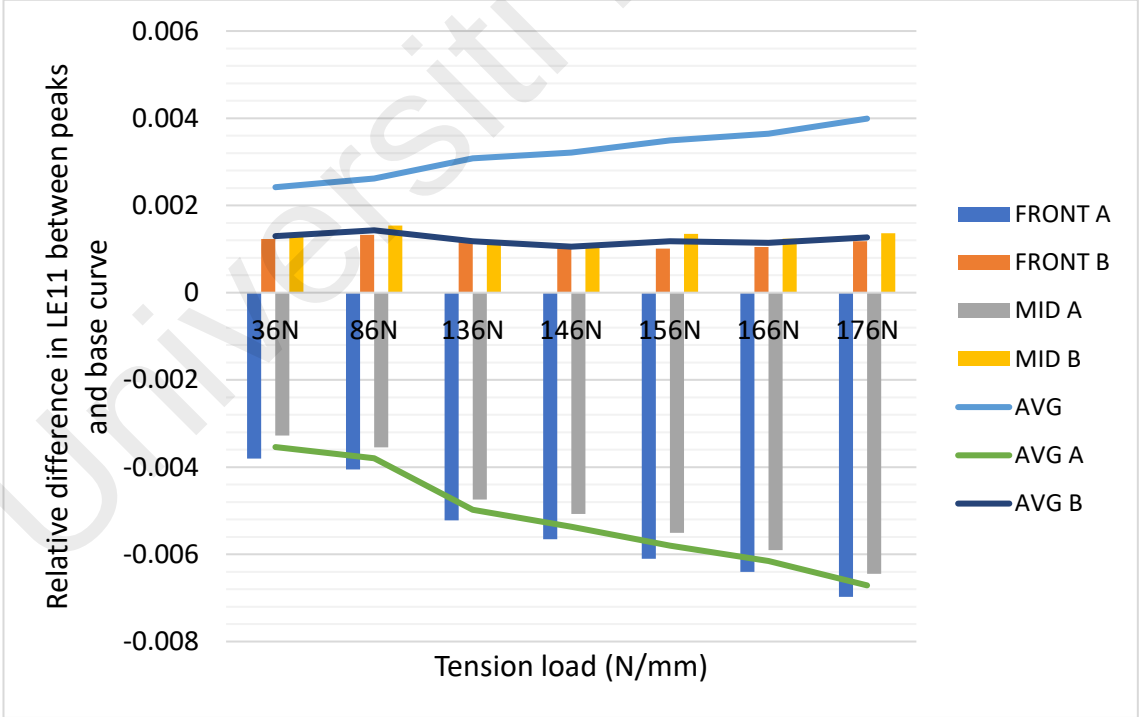

Figure 4.19: Relative difference in LE11 between peaks and valley with base curve on top surface of uncoiled sheets with 1000 mpm at different coil tensions

4.4 Effect of integration points

The effects of integration points in the thickness direction with values of 3, 5 and 7 on simulation accuracy and computational time were investigated in the study as seen in Figure 4.20. The maximum peak and valley heights and the absolute average LE11 strain values in Zone A and Zone B with different integration points were determined and plotted in Figure 4.21. The total computational time of 1000 mpm line speed with 146 N/mm with different integration points was also shown in Figure 4.22.

It could be seen that at higher integration points the LE11 strain value starts to converge. The concentration area of the elements in Zone B2 were found to decrease along with the elimination of islands of tensile strain in Zone B1 at 5 integration points. However, the decrease of concentration area resulted in an overall higher LE11 strain in Zone B2 as compared to 3 integration points. In contrast, the concentration area of Zone B3 starts to significantly increase along with the higher LE11 strain value as shown in Figure 4.20 (b). Hence, the absolute average LE11 strain of Zone B were significantly increased at 5 integration points. The results begin to converge as the absolute average LE11 strain values has no significant changes at 7 integration points as shown in Figure 4.21. The absolute average LE11 strain value in the middle path of Zone B starts to increase with a decrease of LE11 strain in the front path at 7 integration points. This can be explained due to the concentration area of Zone B2 significantly decreased at 7 integration points as shown in Figure 4.20 (c). It can be said that the effect of integration points has more significant effect on the LE11 strain in Zone B. Overall, the LE11 strain values were able to converge at higher integration points as more computational time were required to compute more accurate results. However, the computational time does not vary much as a high-end computer was used to compute the simulation results. The total computational time required for 1000 mpm with 146 N/mm with 7 integration points is 0.38 hours (22.8 mins).

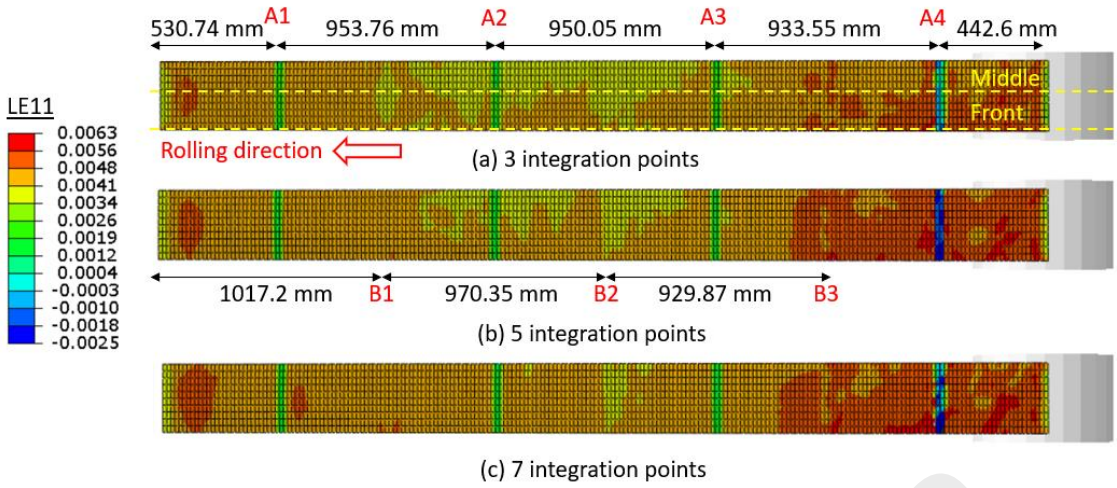

Figure 4.20: True LE11 strain distributions along the top surface of uncoiled sheet at 1000 mpm with 146 N/mm on different integration points.

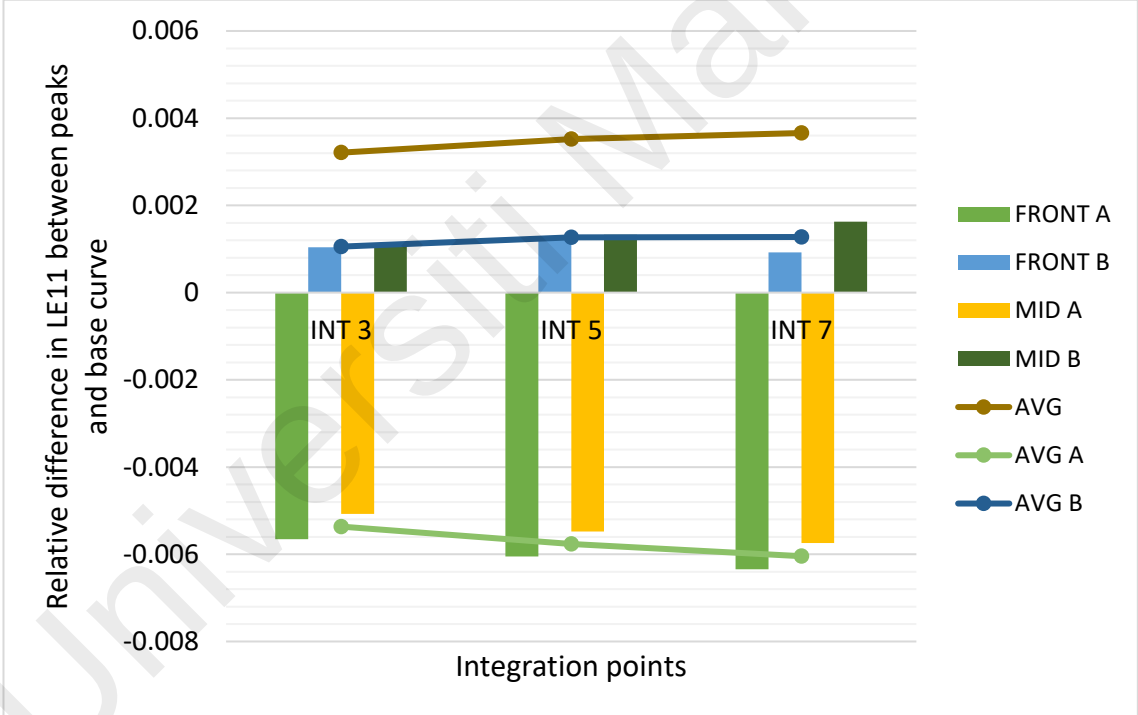

Figure 4.21: Relative difference in LE11 between peak and valley with base curve on top surface of uncoiled sheets at 1000 mpm with 146 N/mm on different integration points

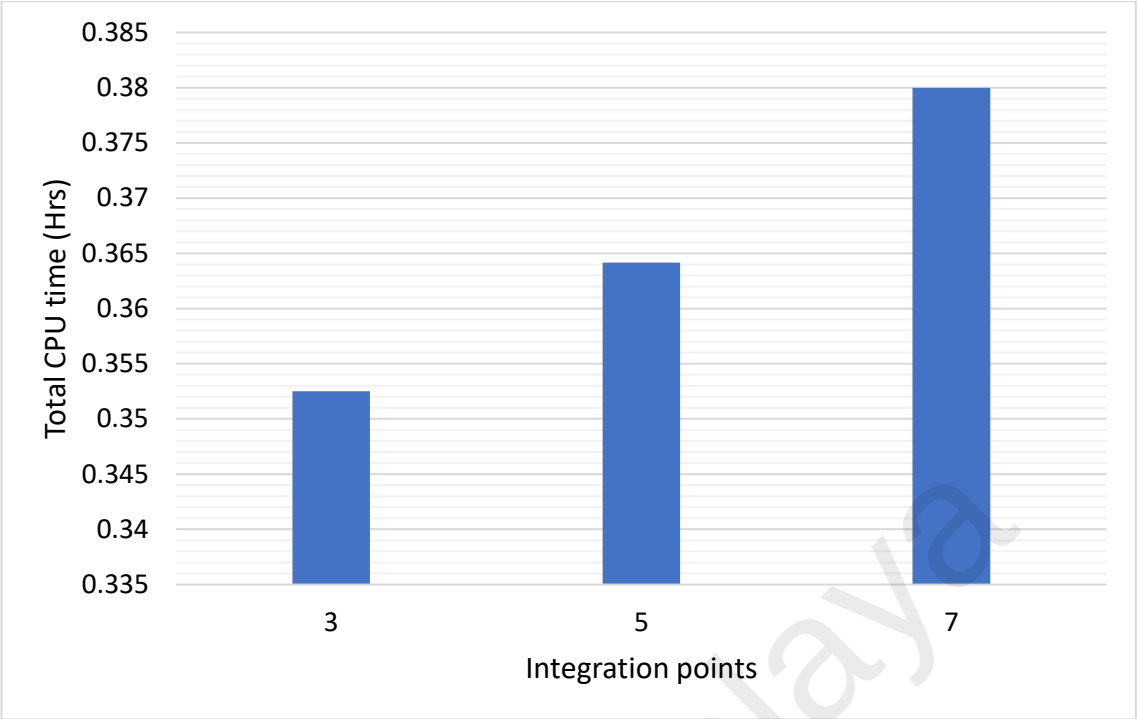

Figure 4.22: Total computational time of 1000 mpm with 146 N/mm on different integration points

CHAPTER 5: CONCLUSIONS AND RECOMMENDATIONS

5.1 Conclusions

The effect of forming speeds on coil break formations during uncoiling of fully annealed low carbon steel sheet were demonstrated with the 3D explicit simulation model. Several parameters such as the coiling tension and integration points were further varied to minimize the coil break formations in the study. The plastic deformation is evidenced by the formation of the interruption zones such as Zone A with narrow band of highly compressive strain and Zone B with islands of tensile strain on the surface of the sheet. Zone A was formed due to localized plastic deformation whereas Zone B were formed due to incomplete plastic unbending.

The coiled sheet was subjected to a high strain rate as it undergoes an increase of line speed. Thus, the severity of the coil break (positive LE11 strain) was observed to be decreasing with increase of line speed. However, the effect of coil tensions on the amount of change of coil break (positive LE11 strain) in Zone B is more significant than the effect of line speed. Therefore, coils tensions are more effective in reducing the coil breaks in Zone B. Overall, the absolute average LE11 strain decreased with high line speed but increased with higher coil tensions. The decrease of the LE11 peak height in Zone A was mainly due to the significant decrease of LE11 strain in the uninterrupted zone at higher speed. Thus, this resulted in the optimum speed of 1000 mpm with the lowest absolute average LE11 strain.

In addition, a rebounded effect was found at coil tension of 146 N/mm with minimum coil break (positive LE11 strain). Thus, 1000 mpm with coil tension of 146 N/mm was chosen as the optimum profile to minimize it. In the mesh analysis with different integration points, the severity of coil breaks formation in Zone B increased along with an increase of highly concentrated compressive strain in Zone A at higher integration

points. This is due to higher accuracy of results with longer computational time could be obtained with more integration points. The total computational time required for 1000 mpm with 146 N/mm with 7 integration points is 0.38 hours (22.8 mins).

5.2 Recommendations

There are some recommendations that can be consider for improvement of future study. Workstation computer such as Intel Xeon processor-based workstation could be used to analyze the coil breaks formation more accurately with the increased number of processors. More accurate stress-strain curves of low carbon steel at different strain rate should be obtained and provided in the simulation settings to improve the accuracy of the simulation results.

Heat transfer analysis should be carried out to determine the effect of annealing conditions such as heating rate, coiling temperature and cooling time on coil break formations during uncoiling. This can be done by the fully coupled thermal-stress analysis in Abaqus software. ACB roll or pressure roll with increased number of coil laps should be included in the simulation to determine the effect on coil break formations. Furthermore, experimental analysis of buckling should be carried out as the highly concentrated compressive strain should be check experimentally for validation whether it is an occurrence of buckling. Geometrical part optimization could be implemented as literature studies suggested that increasing the coil sheet thickness could reduce the severity of coil break.

REFERENCES

Asefi, D., Monajatizadeh, H., Ansaripour, A., & Salimi, A. (2013). Investigation of the effect of skin-pass rolling on the formability of low-carbon steel sheets. *Materiali in Tehnologije*, *47*, 461–466.

Beganović, O., Muminović, B., & Šabanović, M. (2018). *INFLUENCE OF SKIN-PASS ROLLING ON STRENGTH AND DUCTILE PROPERTIES OF EXPLOSIVE WELDED THREE-LAYERS STRIP*.

Callister, W. D., & Rethwisch, D. G. (2015). *Fundamentals of Materials Science and Engineering : An Integrated Approach* (5th edition). Wiley.

Chen, J. K. (2008). Aging Behaviour in Hot-Rolled Low Carbon Steels. *Steel Research International*. Advance online publication. https://doi.org/10.2374/SRI08SP001-79-2008-708

David Llewellyn, & Roger Hudd. (1998). *Steels: Metallurgy and Applications* (3rd ed). Butterworth-Heinemann.

Islam, T., & Rashed, H. M. (2019). Classification and Application of Plain Carbon Steels. In *Reference Module in Materials Science and Materials Engineering*. Elsevier. https://doi.org/10.1016/B978-0-12-803581-8.10268-1

Kobayashi, H. (1999). Origin of Break Marks Produced in the Processing of Mild Steel Strip. In *MECHANICAL WORKING AND STEEL PROCESSING CONFERENCE PROCEEDINGS* (p. 745). Iron and Steel Society.

Melfo, W., Dippenaar, R., & Garten, C. D. (2006). Ridge-buckle defect in thin-rolled steel strip. *Iron and Steel Technology*, *3*, 54–61.

Mucsi, A. (2018). Effect of hot rolling conditions on the nitride precipitation process in low carbon steel strips. *IOP Conference Series: Materials Science and Engineering*, *426*, 12036. https://doi.org/10.1088/1757-899X/426/1/012036

Mucsi, A., Verő, B., & Portász, A. (2016). Coil break formation in low carbon steels. In *Proceedings of Rolling 2016 Conference*.

Mucsi, A. (2018). Analysis of coil break defects. *Engineering Failure Analysis*, *83*, 109–116. https://doi.org/10.1016/j.engfailanal.2017.09.022

Paul, S. K., Ahmed, U., & Megahed, G. M. (2011). Effect of Hot Rolling Process on Microstructure and Properties of Low-Carbon Al-Killed Steels Produced Through TSCR Technology. *Journal of Materials Engineering and Performance*, *20*(7), 1163–1170. https://doi.org/10.1007/s11665-010-9711-4

Paul, S., Raj, A., Biswas, P., Ganapathy, M., & Verma, R. (2014). Tensile flow behavior of ultra low carbon, low carbon and micro alloyed steel sheets for auto application under low to intermediate strain rate. *Materials and Design*, *57*, 211–217. https://doi.org/10.1016/j.matdes.2013.12.047

Shim, D.-S., Son, J.-Y., Lee, E.-M., & Baek, G.-Y. (2017). Improvement strategy for edge waviness in roll bending process of corrugated sheet metals. *International Journal of Material Forming*, *10*(4), 581–596. https://doi.org/10.1007/s12289-016-1303-x

Sun, W., Zhang, X., He, A., & Shao, J. (2016). Research on ridge buckle of high accuracy cold rolled thin strip at local high points during the coiling process. *La Metallurgia Italiana*, *108*, 45–52.

Tan, C. J., & Liew, H. L. (2021). Investigation of coil-break formation during uncoiling of fully annealed low carbon steel sheet using FE simulation. *Engineering Failure Analysis*, *120*, 105112. https://doi.org/10.1016/j.engfailanal.2020.105112

Thakur, S. K., Sarkar, B., Ghosh, B., & Datta, R. (2014). Reduction in diversion due to coil break in CRNO grades of coils. *Case Studies in Engineering Failure Analysis*, *2*(2), 76–83. https://doi.org/10.1016/j.csefa.2014.04.005

Wendt, P., Frech, W., & Leifgen, U. (2007). Cold rolling defect,"stickers" and countermeasures. *Heat Processing*, *2*, 127–135.

Zhou, T., Zurob, H., Zhang, P., Kuuskman, K., Cho, S. H., & Burella, D. (2019). Control of edge breaks during cold mill processing of commercial and drawing quality low-carbon steels. *Ironmaking & Steelmaking*, *46*(7), 656–662. https://doi.org/10.1080/03019233.2018.1440780